



Sedimentary Mo isotope variability reflects climate-driven water column oxygenation changes in ferruginous Lake Towuti, Indonesia over the last ~30 ka BP

Adrianus Damanik ^{a,b,c,*}, Martin Wille ^a, Qasid Ahmad ^d, Sean A. Crowe ^{e,f}, Kohen W. Bauer ^g, Martin Grosjean ^{b,h}, Sri Yudawati Cahyarini ^c, Satria Bijaksana ⁱ, James M. Russell ^j, Hendrik Vogel ^{a,b}

^a Institute of Geological Sciences, University of Bern, Baltzerstrasse 1+3, CH-3012, Bern, Switzerland

^b Oeschger Center for Climate Change Research, University of Bern, Hochschulstrasse 4, CH-3012, Bern, Switzerland

^c Paleoclimate & Paleoenvironment Research Group-Research Center of Climate and Atmosphere, National Research and Innovation Agency (BRIN), Jalan Sangkuriang, ID-40135, Bandung, Indonesia

^d Centre de Recherches Pétrographiques et Géochimiques (CRPG), CNRS, UMR, 7358, Nancy, France

^e Department of Earth, Ocean, and Atmospheric Sciences, University of British Columbia, Health Sciences Mall, CA-2350, Vancouver, Canada

^f Department of Microbiology and Immunology, University of British Columbia, Health Sciences Mall, CA-2350, Vancouver, Canada

^g Ocean Networks Canada, University of Victoria, Ocean-Climate Building #100, 2474 Arbutus Road, Victoria, BC, Canada

^h Institute of Geography, University of Bern, Hallerstrasse 12, CH-3012, Bern, Switzerland

ⁱ Faculty of Mining and Petroleum Engineering, Institut Teknologi Bandung, Jalan Ganesha 10, ID-40132, Bandung, Indonesia

^j Department of Earth, Environmental, and Planetary Sciences, Brown University, 324 Brook St., 02912, Providence, RI, USA

ARTICLE INFO

Handling editor: Mira Matthews

Keywords:

Water column oxygenation

Molybdenum isotopes

Fe oxides

Organic matter

Lake mixing

Lake Towuti

ABSTRACT

Previous studies have shown the utility of Molybdenum (Mo) concentrations and isotopic compositions as sensitive recorders for changes in redox conditions in marine environments. Compared to marine settings, the much lower dissolved Mo concentrations in freshwater settings could result in enhanced sensitivity of Mo isotopic composition to the temporal variability in redox conditions. Additionally, unlike the dissolved Mo isotopic compositions in open marine environments, freshwater settings are highly influenced by site-specific factors such as catchment characteristics and in-lake processes. Here, we present sedimentary Mo concentration ([Mo]) and isotope ($\delta^{98}\text{Mo}$) data from presently stratified Lake Towuti (Indonesia) to provide insight into Mo behaviour in ferruginous (Fe-rich) and non-sulfidic freshwater settings. We find large variations in [Mo] (0.12–1.11 $\mu\text{g g}^{-1}$) and $\delta^{98}\text{Mo}$ (−0.14 ‰ to −1.13 ‰) in lake surface sediments, which are distinct from previously reported variations found in weathering profiles of the ultramafic catchment. The [Mo] variation can partly be attributed to hydrodynamic sorting, with Mo enrichment at pelagic deep water sites distant from the major lake inflows. Sedimentary $\delta^{98}\text{Mo}$ shows a distinct pattern, with generally higher values in sediments deposited in deep anoxic water compared to lower $\delta^{98}\text{Mo}$ values in sediments deposited in shallow water sites above the oxycline. We attribute this $\delta^{98}\text{Mo}$ pattern in Lake Towuti predominantly to redox-controlled processes. These involve the reductive dissolution of suspended laterite-sourced Fe oxides, with Mo liberation under anoxic conditions shortly below the sediment-water interface and/or water column oxycline. Above the oxycline, the formation of amorphous Fe oxides promotes the preferential adsorption of isotopically light Mo. This partial scavenging of isotopically light Mo leads to the formation of isotopically heavier dissolved Mo reservoirs. The scavenging of isotopically heavy dissolved Mo by organic matter (OM) coupled with higher OM burial rates in anoxic sediments promotes higher sedimentary $\delta^{98}\text{Mo}$ ratios in sediment deposited below the oxycline, where OM is better preserved and amorphous Fe oxides are preferentially dissolved. When applying this framework of modern lake processes to a sediment piston core extending back ~30 ka, we find $\delta^{98}\text{Mo}$ variations that are similar to those observed in modern surface sediments, both above and below the oxycline. Low $\delta^{98}\text{Mo}$ values in sediments deposited between ~30 and ~14 cal ka BP suggest deep oxygenation of the water column to the sediment-water interface. In contrast, Mo isotope signatures between ~14 cal ka BP and the present are similar to those of

* Corresponding author. Institute of Geological Sciences, University of Bern, Baltzerstrasse 1+3, CH-3012, Bern, Switzerland.

E-mail address: adrianus.damanik@unibe.ch (A. Damanik).

present-day deep water anoxic sites, suggesting water column stratification throughout the Holocene. The water column oxygenation pattern inferred from $\delta^{98}\text{Mo}$ aligns well with other independent sedimentary indicators that indicate a cooler, drier last glacial maximum with deep water column mixing, and a warmer, wetter Holocene with a stratified water column. Thus, our results imply that $\delta^{98}\text{Mo}$ can be applied as an effective tracer of climate-driven changes in water column oxygenation in ferruginous and non-sulfidic settings.

1. Introduction

Climate parameters such as temperature, solar and longwave radiation, evaporation, and wind stress play a key role in controlling lake water column mixing (Boehrer and Schultze, 2008). Variations of these parameters can significantly influence the frequency and intensity of mixing events and the depth to which mixing extends within the water column (Cannon et al., 2021; Fukushima et al., 2017). Mixing events drive redox-controlled cycling processes that alter the nutrient and redox-sensitive element composition within the water column and facilitating exchange with sediments (Boehrer and Schultze, 2008). Consequently, oxidation and reduction cycling result in characteristic sedimentary element concentration and isotopic compositions which can be utilized to track climate-driven changes in water column oxygenation (Brown et al., 2000; Costa et al., 2015; Katsev et al., 2010; Makri et al., 2021; Zander et al., 2021).

Sedimentary molybdenum concentrations ([Mo]) and isotope ratios ($\delta^{98}\text{Mo}$, relative to NIST SRM 3134 = 0 ‰ in this study) are well-known and useful indicators of past redox changes in the oceans, where they have been applied to sediment records to trace long-term changes in Earth's oxygenation history (Algeo and Lyons, 2006; Arnold et al., 2004; Barling et al., 2001; Kendall et al., 2017; Lyons et al., 2014; Pearce et al., 2008; Siebert et al., 2003; Wille et al., 2007, 2013). For instance, Mo isotopic signatures in marine sediments have been widely used to track global marine redox changes during the two major oxidation events at the Archean-Paleoproterozoic boundary and the Precambrian-Cambrian transition (Duan et al., 2010; Kurzweil et al., 2015; Siebert et al., 2005; Voegelin et al., 2010; Wille et al., 2007). The Mo isotopic composition in marine sediments has also been used as a proxy to understand the extent of oceanic deoxygenation, such as during Phanerozoic Ocean Anoxic Events (OAEs; Dahl et al., 2019; Pearce et al., 2008; Poulsen et al., 2006; Siebert et al., 2021, 2003).

Although sedimentary records of [Mo] and $\delta^{98}\text{Mo}$ are widely recognized as redox change proxies in marine settings, our understanding of the processes governing Mo isotope signatures and cycling in freshwater (lacustrine) settings remains comparatively limited. Nevertheless, the processes and conditions that affect Mo speciation and isotope fractionation in lacustrine settings can be expected to be similar to those observed in marine settings. Under oxic conditions, Mo is typically present as soluble molybdate (MoO_4^{2-}). Adsorption of MoO_4^{2-} onto Mn oxides (and Fe oxides) can exert a large control on dissolved Mo concentrations and isotopic composition (Barling et al., 2001). The preferential adsorption of lighter Mo isotopes onto these oxides can serve as an indicator of oxic conditions during sediment deposition (Barling and Anbar, 2004; Goldberg et al., 2012; Kashiwabara et al., 2011; Malinovsky et al., 2007; Scott and Lyons, 2012). However, early diagenetic processes at the redox interfaces can later affect the Mo concentration and isotope compositions in open waters and/or sediments (Canfield et al., 1993). Under euxinic water conditions, in the presence of free H_2S , thiomolybdate species are formed (Helz et al., 2011). Higher thiomolybdate particle reactivity and more efficient scavenging of dissolved Mo (Mo_{diss}) under euxinic conditions lead to two to three orders of magnitude higher Mo concentrations in marine sapropels compared to sediments deposited under oxic bottom water conditions (Bertine and Turekian, 1973; Helz et al., 2011). Under strong euxinic bottom water conditions with $\text{H}_2\text{S}_{\text{aq}} > 11 \mu\text{M}$, near quantitative Mo_{diss} removal leads to a transfer of the Mo isotopic seawater signature into the marine sediment (Nägler et al., 2011; Neubert et al., 2008).

However, MoO_4^{2-} removal is not only a function of $\text{H}_2\text{S}_{\text{aq}}$ concentration, but is also influenced by interactions with Fe(II) sulfides, organic matter (OM), and deep-water residence time, which together affect the drawdown of Mo from euxinic water columns and its isotope composition in the sediment (Algeo and Lyons, 2006; Helz et al., 2011).

While the behaviour of Mo and its stable isotope compositions in euxinic as well as in hypoxic marine settings has been investigated (Brucker et al., 2009; Hardisty et al., 2016; Nägler et al., 2011; Neubert et al., 2008; Scholz et al., 2018), its cycling in ferruginous, low-sulfur settings remains poorly constrained. Regardless, these conditions were likely widespread throughout the Earth's early oceans with lower atmospheric oxygen concentration and the persistence of ocean redox stratification limiting the accumulation of sulfate in the ocean (Planavsky et al., 2011; Poulton and Canfield, 2011). Due to the absence of these conditions in modern marine settings, ferruginous lakes have been suggested as potentially suited modern analogs to investigate element cycling under ferruginous conditions (Bauer et al., 2018; Busigny et al., 2014; Janssen et al., 2024; Swanner et al., 2020; Vuillemin et al., 2022).

Aside from the presence of Mn-oxides, the mobility of Mo is fundamentally linked to redox transitions of S and Fe in both marine and freshwater settings (Kendall et al., 2017). In ferruginous, low-sulfur lacustrine settings, the absence of free sulfide alters Mo removal pathways and stable isotope compositions across interconnected reservoirs (e.g. water column - sediment) (Scholz et al., 2017) (citation). Unlike sulfidic settings, where Mo complexes associate with sulfurized OM, removal in ferruginous settings is expected to be primarily mediated by Fe (oxyhydr)oxides, which preferentially adsorb isotopically light Mo (Goldberg et al., 2009). This potential process should result in distinct isotopic signatures not directly comparable to marine euxinic pathways. Coupled Fe-Mo sedimentary enrichment and covariation in porewater, such as those observed in Peruvian shelf sediments, have been interpreted as evidence of Mo delivery to surface sediments via an Fe (oxyhydr)oxide shuttle (Scholz et al., 2017). Such shuttling can influence Mo isotope compositions in settings where dissolved Mn is low (Goldberg et al., 2012). Overall, in ferruginous settings, Mo is expected to be effectively removed from solution mainly by adsorption onto Fe (oxyhydr)oxides and OM, in which both processes favor the retention of isotopically light Mo (Goldberg et al., 2012; King et al., 2018).

Moreover, while redox processes are still anticipated to control Mo isotope fractionation, other factors may exert a more prominent influence in lacustrine settings. Given the low reservoir size and low residence time of dissolved Mo in these environments, variations in Mo input from diverse sources, changing biological productivity and OM flux may significantly affect Mo cycling and must be thoroughly assessed. For example, variations in Mo isotopic composition may be caused by site-specific factors such as bedrock compositions and chemical weathering of bedrock substrates as well as anthropogenic sources of Mo (Chappaz et al., 2012; Damanik et al., 2024; Malinovsky et al., 2007). An example of the Mo heterogeneity in lacustrine sedimentary records originates from meromictic and sulfidic Lake Cadagno, Switzerland (Dahl et al., 2013), where dissolved Mo exhibits distinct isotope signatures between the upper oxygenated and lower sulfidic water column, coinciding with lower and higher Mo concentrations, respectively. This difference has been attributed to variations in $\delta^{98}\text{Mo}$ from surface and groundwater sources, and the removal of isotopically light Mo into sediments under sulfidic conditions (Dahl et al., 2010, 2013; Wirth et al., 2013). This shows that different catchment

characteristics and changes in-lake processes can influence Mo cycling in lakes, highlighting the need for a thorough assessment of these factors. Once the dependence of the Mo cycle on these site factors is determined, downcore sediment Mo variability can be utilized to track changes in environmental parameters back in time. Hence, to fully utilize the potential of Mo as a water column oxygenation proxy and its main drivers in diverse lacustrine settings, it is essential to comprehensively investigate different lacustrine endmember environments.

Here we investigate the behaviour of Mo in thermally stratified, ferruginous and low-sulfur Lake Towuti on Sulawesi, Indonesia. The site-specific Mo mobility during weathering has been previously discussed using $\delta^{98}\text{Mo}$ data from Lake Towuti's ultramafic catchment of the

East Sulawesi Ophiolite, which is overlain by thick lateritic soils (Damanik et al., 2024). Seasonal mixing maintains oxygenation of the upper ~100 m of the water column in modern Lake Towuti and is closely tied to climate, with deep mixing occurring during the dry season primarily due to enhanced evaporative cooling of surface waters (Costa et al., 2015; Pu et al., 2025). During the last glacial maximum, when the climate around Lake Towuti was substantially cooler and drier (Parish et al., 2023, 2024; Russell et al., 2014; Zhao et al., 2023) and the lake level was lower (Tournier et al., 2023; Vogel et al., 2015), sedimentary and geochemical indicators suggest deeper mixing with oxygenation of the entire water column (Costa et al., 2015; Morlock et al., 2019; Russell et al., 2020; Sheppard et al., 2019). With its limnologically and

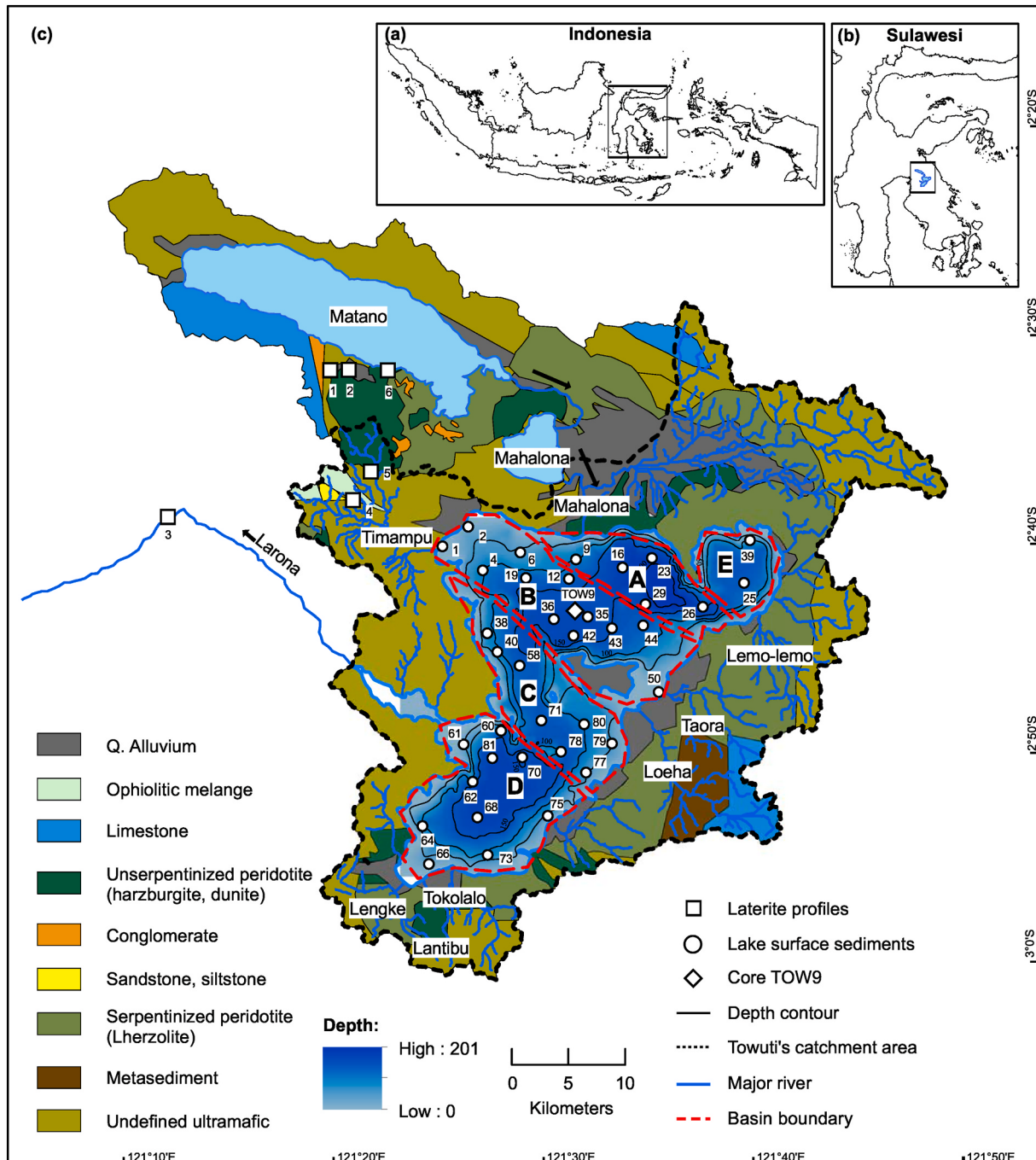


Fig. 1. (a) Map of Indonesia, (b) Map of Sulawesi Island, and (c) Geological map (modified from Costa et al., 2015) of the Malili Lake System catchment area. The catchment area of Lake Towuti (Morlock et al., 2019), with the sampling locations used in this study, is in the south of the Malili Lake System. Laterite profile sampling points are from Damanik et al. (2024). The labels A-E in Lake Towuti are the five basins delineated by presumed faults (Tournier et al., 2023).

geochemically unique characteristics and history of climate-forced changes in water column oxygenation, Lake Towuti provides an ideal target to investigate the behavior of Mo in a ferruginous environment containing overall low concentrations of dissolved Mo and S. For this, we investigate Mo concentrations and isotope ratios in surface sediment samples from Lake Towuti, collected at various depths above and below the oxycline, to identify the allochthonous factors and in-lake processes governing modern Mo deposition. We then apply these findings to a continuous sediment piston core from Lake Towuti, spanning the last ~30 ka, to explore the potential of Mo as a water column (de-)oxygenation proxy. These findings are assessed alongside available climate, weathering, transport, depositional, and redox proxy records from the same sediment core (Costa et al., 2015; Morlock et al., 2019; Russell et al., 2014, 2020; Sheppard et al., 2019; Vogel et al., 2015).

2. Regional settings

Lake Towuti, a 560 km² large and up to ~200 m deep tectonic lake is located in East Sulawesi, Indonesia and is estimated to be > 1 Myr old (Russell et al., 2020). The catchment occupies an area of 1286 km² and encompasses upstream lakes Matano and Mahalona with Lake Towuti draining into the Bay of Bone (Fig. 1). The northwestern part of the catchment includes upstream lakes Matano and Mahalona. The northern part includes relatively wide and flat valleys, whereas the northeastern and southwestern parts are characterised by steep slopes up to 67° with direct drainage into the lake (Morlock et al., 2019, Fig. 1; S1). The catchment is predominantly composed of ultramafic dunites, lherzolites, and harzburgites of the East Sulawesi Ophiolite with minor occurrences of metasedimentary successions with more felsic composition in the eastern part of the catchment (Fig. 1; Costa et al., 2015; Kadarusman et al., 2004; Morlock et al., 2019). Throughout the catchment, the bedrock is deeply weathered with thick lateritic soils covering the bedrock and providing erodible materials with high concentrations of Fe and other metals (Golightly, 1979; Hasberg et al., 2019; Morlock et al., 2019). High input of Fe oxyhydroxides from the laterites into the lake leads to ferruginous (up to ~10 µM), low sulfate (SO₄²⁻ = 15.6–21 µM), and ultraoligotrophic conditions in Lake Towuti (Costa et al., 2015; Lehmusluoto and Machbub, 1997).

The region's climate is humid tropical with a 26 °C mean annual air temperature and an annual precipitation amount of ~2700 mm. Peak rainfall (~330 mm/month) occurs in austral autumn (March–May) and comparatively dry conditions (~140 mm/month) prevail during the austral spring months (August–October; Konecky et al., 2016). Modern lake surface temperature monitoring in 2012–2013 shows seasonal mixing in Lake Towuti's water column is evident at ~90 m water depth due to the evaporative cooling and enhanced heat loss during the dry season (Costa et al., 2015). The water temperature remains nearly constant at 28.4 °C below ~90 m water depth, indicating a lack of annual mixing in the deeper layer, for the observation period. This results in an anoxic water column below 140 m water depth, with hyposalinidic conditions. Nevertheless, Costa et al. (2015) highlighted that extended and more extreme dry seasons could potentially cause changes in the depth of lake mixing, allowing the complete lake mixing and thus increasing oxygen availability in the bottom water of Lake Towuti.

Lake Towuti is separated into five sub-basins by fault-controlled subaqueous ridges (Fig. 1; Russell et al., 2020; Tournier et al., 2023). The northern basins A and B receive substantial sediment input characterized by high concentrations of serpentine minerals and Mg from the Mahalona River, Towuti's largest inlet (Fig. 1; Hasberg et al., 2019). The remainder of the rivers providing sediment inputs to the northern basins A and B are substantially smaller. The Loeha River, the second largest inlet, albeit substantially smaller compared to the Mahalona, drains a catchment which provides inputs with a more felsic composition, also contributing to the sediment input in basins A and B (Hasberg et al., 2019; Morlock et al., 2019). However, the majority of the Loeha

suspended sediment input is diverted into the southwestern basin C (Hasberg et al., 2019; Morlock et al., 2019). Catchments in the southwest and northeast providing sediment input to basins D and E (Fig. 1), are drained by smaller rivers and creeks. Catchments surrounding Basin E and the western parts of Basins C and D are predominantly characterized by steep and deeply incised terrain with frequent landslides (Morlock et al., 2019; Tournier et al., 2023, Fig. 1, S1). The Fe-rich composition of the lake surface sediments in these basins has been interpreted as originating from the more direct input of lateritic soil substrates as a result of a predominance of gully erosion and frequent mass wasting (Fig. S1; Morlock et al., 2019; Tournier et al., 2023).

3. Materials and methods

3.1. Sediment sampling and auxiliary data

Molybdenum isotope and elemental analyses were performed on a set of samples collected in 2010 and 2015, including lake surface sediments from various locations in the lake, and a ~10-m-long piston core IDLE-TOW10-9B-1K (abbreviated TOW9; Fig. 1). To assess the factors controlling modern Mo deposition, 37 lake surface sediment samples (Hasberg et al., 2019; Morlock et al., 2019) were selected in a spatially explicit approach to encompass a range of water depths (4–178 m water depth) and from all of the five different subbasins (Fig. 1; Table 1; Tournier et al., 2023). Sediment core TOW9, recovered from 154 m water depth in the northern basin, is generally unaffected by event deposition and has been extensively studied (Costa et al., 2015; Konecky et al., 2016; Morlock et al., 2019; Russell et al., 2014). Given its location below the modern oxycline, TOW9 is also ideal for better understanding the effects of climate-driven redox changes (Costa et al., 2015; Sheppard et al., 2019). Core TOW9 was sampled systematically for the portion of the record spanning the past ~30 ka using a ~1.5 ka sampling resolution. The TOW9 chronology is based on radiocarbon dating calibrated to Intcal20 (Parish et al., 2023). All sediment samples were freeze-dried and homogenized to a fine powder using an agate mortar and pestle. Samples (~1 g) were heated to 600 °C for 6 h to remove OM prior to Mo purification.

3.2. Mo purification and isotope measurements

Mo separation and isotope analysis were performed in the clean laboratory facilities at the Institute of Geological Sciences, University of Bern. Depending on the Mo concentration of the samples, powdered aliquots were weighed into pre-cleaned 7 or 14 ml Savillex™ Teflon beakers to match 25–50 ng of total Mo and spiked with an appropriate isotope tracer solution enriched in ⁹⁷Mo and ¹⁰⁰Mo (Siebert et al., 2001). Sample dissolution was achieved through sequential digestion steps using a single-distilled HF - HNO₃ mixture (3:1) for at least 48 h followed by digestion with 6 M HCl at least twice. During the dissolution in HF-HNO₃ and HCl, the beakers were placed on a hotplate at 80 °C and 120 °C, respectively.

Mo was purified using a sequence of anion and cation exchange resins. All the chemical separations were performed following procedures reported by (Ahmad et al., 2023; Damanik et al., 2024; Wille et al., 2013). In brief, samples were dissolved in 3 ml 4 M HCl + 0.15 % H₂O₂ before being loaded into a single column with 2 cm³ anion exchange resin Dowex AG 1X8 (200–400 mesh) for chemical separation. For further chemical separation, samples were prepared in 2 ml 0.5 M HCl + 0.1 % H₂O₂ before being loaded into a single column with 2 ml cation exchange resin Dowex 50X8 (200–400 mesh). Purified Mo was dissolved in 1 ml 0.5 M HNO₃ before the isotope composition measurement.

Isotopic compositions were measured on a ThermoFisher Scientific NeptunePlus multicollector inductively coupled plasma mass spectrometer (MC-ICP-MS) coupled with an Aridus II desolvating nebulizer. Six Mo isotopes (⁹⁴Mo, ⁹⁵Mo, ⁹⁶Mo, ⁹⁷Mo, ⁹⁸Mo, and ¹⁰⁰Mo) were measured as well as ⁹⁹Ru and ¹⁰¹Ru to monitor isobaric interference. We

Table 1

[Mo] ($\mu\text{g}\cdot\text{g}^{-1}$) and $\delta^{98}\text{Mo}$ (%) of lake surface sediments and core TOW 9 with other relevant parameters. Ti, Fe, Al, TOC, and clay content of lake surface sediments are available from Hasberg et al. (2019) and Morlock et al. (2019). Samples from lake surface sediments are divided based on the basin (Tournier et al., 2023) and core sediment is divided based on the epoch.

Sample ID	Depth (m) ^a	Age (cal ka BP)	Mo ($\mu\text{g}\cdot\text{g}^{-1}$)	$\delta^{98}\text{Mo}$ (%)	2SE (%) ^b	Ti (%)	Fe (%)	Al (%)	TOC (%)	Clay (%)
Lake Surface Sediments										
Basin A										
Surf9	96.4	–	0.23	-0.53	0.025	0.16	9.24	3.18	3.56	0.16
Surf16	174.9	–	0.47	-0.33	0.026	0.16	10.1	3.51	5.99	0.15
Surf23	177.9	–	0.85	-0.31	0.021	0.2	15	4.64	4.31	0.31
Surf26	137.7	–	0.76	-0.42	0.020	0.23	17.3	5.35	3.47	0.38
Surf29	172.1	–	1.04	-0.38	0.023	0.23	14.6	5.38	4.09	0.33
Basin B										
Surf1	6.3	–	0.45	-1.13	0.021	0.23	10.1	6.67	2.41	0.17
Surf2	5.4	–	0.55	-0.80	0.021	0.19	11.6	7.26	3.13	0.17
Surf4	97.5	–	0.74	-0.50	0.022	0.35	13.3	5.84	3.47	0.35
Surf6	7.5	–	0.35	-0.73	0.024	0.24	7.91	6.45	2.16	0.06
Surf12	124.7	–	0.44	-0.35	0.023	0.21	10.5	4.14	3.00	0.23
Surf19	123.7	–	0.87	-0.39	0.023	0.34	13.8	5.88	3.41	0.31
Surf35	154	–	0.73	-0.26	0.023	0.22	13.3	5.02	4.01	0.25
Surf36	157.7	–	0.74	-0.35	0.024	0.24	12.9	5.33	3.96	0.28
Surf42	161.8	–	0.85	-0.30	0.019	0.24	13.4	5.61	4.24	0.30
Surf43	141.6	–	0.93	-0.30	0.023	0.23	14	5.45	4.30	0.31
Surf44	126.8	–	0.66	-0.36	0.025	0.29	15	6.47	3.30	0.29
Surf50	4.5	–	0.12	-0.53	0.027	0.06	12.1	2.29	0.17	0.03
Basin C										
Surf38	78.5	–	0.80	-0.31	0.021	0.29	15	6.37	3.74	0.35
Surf40	101.2	–	0.88	-0.35	0.020	0.28	15.2	6.21	3.67	0.37
Surf58	127.6	–	0.85	-0.42	0.019	0.27	13.8	6.22	4.00	0.36
Surf71	132	–	0.85	-0.40	0.018	0.34	12	7.76	3.12	0.34
Surf77	53.4	–	0.60	-0.38	0.022	0.39	11.4	7.53	5.55	0.23
Surf78	119	–	0.82	-0.44	0.031	0.37	12	8.68	2.77	0.33
Surf79	46.8	–	0.31	-0.39	0.017	0.24	6.5	5.59	1.39	0.10
Surf80	99.8	–	0.63	-0.51	0.015	0.41	10.9	8.5	2.60	0.27
Basin D										
Surf60	134.3	–	1.11	-0.35	0.033	0.2	19.2	5.5	5.52	0.43
Surf61	117.6	–	1.05	-0.34	0.022	0.2	20.8	5.86	4.94	0.32
Surf62	117.5	–	0.95	-0.42	0.017	0.25	18.6	6.71	4.45	0.41
Surf64	77.5	–	0.87	-0.26	0.019	0.19	21.4	5.64	4.66	0.38
Surf66	40.7	–	0.41	-0.14	0.032	0.06	28.9	3.45	4.06	0.07
Surf68	168.8	–	1.01	-0.39	0.024	0.24	17	6.61	3.07	0.40
Surf70	152	–	0.92	-0.51	0.016	0.37	17.8	9.08	3.47	0.39
Surf73	87.1	–	0.89	-0.26	0.020	0.24	18.9	6.47	1.97	0.29
Surf75	50.6	–	0.51	-0.32	0.021	0.26	15.3	5.77	2.55	0.19
Surf81	168.5	–	0.84	-0.35	0.029	0.23	19.3	6.06	5.27	0.42
Basin E										
Surf25	129.2	–	0.94	-0.20	0.024	0.16	21	4.31	6.43	0.32
Surf39	101.1	–	0.90	-0.16	0.021	0.15	20.6	4.44	5.93	0.34
Core TOW 9										
Green Clay										
TOW 9-1 24–26 cm	0.25	1.2	0.95	-0.22	0.017					
TOW 9-1 63–66 cm	0.65	3.1	0.64	-0.26	0.016					
TOW 9-2 43.5–45 cm	1.09	6.0	0.41	-0.27	0.016					
TOW 9-3 16.5–19 cm	1.44	7.2	0.58	-0.25	0.021					
TOW 9-3 46–48 cm	1.74	8.0	0.49	-0.28	0.014					
TOW 9-3 68.5–71 cm	1.96	8.8	0.62	-0.14	0.018					
TOW 9-3 81–83 cm	2.09	9.5	0.91	-0.14	0.018					
TOW 9-3 91–93 cm	2.19	10.4	0.55	-0.43	0.021					
TOW 9-4 4–6 cm	2.29	11.7	0.54	-0.36	0.019					
TOW 9-4 34–36 cm	2.59	13.9	0.56	-0.39	0.021					
TOW 9-4 66–68 cm	2.91	15.8	0.33	-0.49	0.023					
Sideritic Clay										
TOW 9-4 96–98 cm	3.21	17.2	0.29	-0.45	0.026					
TOW 9-4122–124 cm	3.47	18.4	0.24	-0.41	0.036					
TOW 9-5 16–18 cm	3.80	20.1	0.27	-0.47	0.026					
TOW 9-5 46–48 cm	4.10	21.4	0.30	-0.52	0.020					
TOW 9-5 85.5–88 cm	4.50	23.3	0.31	-0.49	0.026					
TOW 9-6 27–29 cm	4.83	25.0	0.22	-0.67	0.027					
TOW 9-6 56–58 cm	5.12	26.4	0.19	-0.56	0.027					
TOW 9-6 94–96.5 cm	5.50	28.2	0.37	-0.57	0.022					
TOW 9-6126–128 cm	5.82	29.5	0.36	-0.36	0.022					

^a water depth (m) for the lake surface sediments, depth (m) from the top for core TOW 9.

^b 2 standard error of the measurement (80 cycles at 4.194 s integration time).

used faraday cups with $10^{11} \Omega$ to analyze all isotopes except ^{101}Ru , which was measured using a $10^{12} \Omega$ resistor. For analyses, we have used a combination of a standard 'H' Ni sampler cone and an 'X' Ni skimmer cone and obtained $\sim 28 \text{ V/ppm}$ on ^{95}Mo . Mo concentrations were obtained by the inverse isotope dilution method from the double-spike deconvolution. Mo isotope ratios were calculated using the double-spike correction method (Siebert et al., 2001) and reported as parts per thousand deviations of $^{98}\text{Mo}/^{95}\text{Mo}$ of the sample relative to NIST SRM 3134 = 0 ‰ with an interference correction based on simultaneously measured $^{99}\text{Ru}^+$. Repeated measurements of the in-house Johnson Matthey standard solution lot 602332B ("JMCBern"; Siebert et al., 2001) gave an isotopic difference of 0.263 ± 0.011 ‰ $\delta^{98}\text{Mo}$ (2SD, $n = 21$) relative to NIST SRM 3134 (Goldberg et al., 2013) in agreement with previous studies (Ahmad et al., 2021, 2022, 2023; Damanik et al., 2024; Greber et al., 2012). Background correction was applied by averaging background intensities of pure 0.5 M HNO₃ carrier solution that was measured on-peak before and after the analysis of every sample. Sample and background analysis consisted of 80 and 30 cycles, respectively, with a signal integration time of 4.194 s for each cycle. The Mo blank of the chemical procedures was $< 0.52 \text{ ng}$.

Analyses of individually digested and chemically purified AGV-2, BHVO-2, W-2a, and BIR-1a whole-rock reference materials yielded $\delta^{98}\text{Mo}$ values of -0.18 ± 0.04 ‰ (2SD; $n = 5$), -0.10 ± 0.04 ‰ (2SD; $n = 2$), -0.06 ± 0.05 ‰ (2SD; $n = 5$), and -0.15 ± 0.06 ‰ (2SD; $n = 2$), respectively, which is in agreement with values previously determined (Fan et al., 2020; Feng et al., 2020; Willbold et al., 2016; Zhao et al., 2016). Individual measurements of geological whole-rock reference materials can be found in [Supplementary Material Table S1](#). Repeated measurement of W-2a documents a long-term 2SD reproducibility of ± 0.05 ‰, which we consider to be the reproducibility of measurements of samples. This is in line with previous in-house measurements of AGV-2 (-0.18 ± 0.05 ‰; 2SD; $n = 5$; Damanik et al., 2024) and BHVO-2 (-0.09 ± 0.05 ‰, 2SD; $n = 13$; Ahmad et al., 2023, 2022, 2021) analyzed at the Institute of Geological Sciences, University of Bern.

4. Results

4.1. [Mo] and $\delta^{98}\text{Mo}$ variability of lake surface sediments

The [Mo] and $\delta^{98}\text{Mo}$, as well as concentrations for other constituents discussed below (Al, Ti, Fe, TOC, and clay content), are listed in [Table 1](#). The [Mo] in lake surface sediments ranges from 0.12 to 1.11 $\mu\text{g}\cdot\text{g}^{-1}$ ([Fig. 2a](#)). The lowest [Mo] occurs near major inlets, especially around the Mahalona, Loeha, Taora, and Lengke Rivers. Mo concentration generally increases with greater distance from the major inlets ([Fig. 2a](#)). In contrast, samples from the northeastern basin E and southwestern basins C and D show a more homogeneous and elevated [Mo] pattern without discernible influence of distance to the shoreline ([Fig. 2a](#)).

The $\delta^{98}\text{Mo}$ of lake surface sediments ranges from -0.14 ‰ to -1.13 ‰ ([Fig. 2b](#)). Surface sediments from deeper parts below the current oxycline ($> 140 \text{ m}$ water depth) in the larger basins A and B exhibit higher $\delta^{98}\text{Mo}$ values compared to those collected from above the oxycline. A lake surface sediment sample taken close to the shoreline has the lowest $\delta^{98}\text{Mo}$ value (-1.13 ‰) in the dataset. In contrast, sediments from the smaller basins C, D, and E do not show significant differences in $\delta^{98}\text{Mo}$ for sediments originating from below and above the oxycline.

4.2. [Mo] and $\delta^{98}\text{Mo}$ variability in sediment core TOW9

The [Mo] and $\delta^{98}\text{Mo}$ in core TOW9 range from 0.19 to 0.95 $\mu\text{g}\cdot\text{g}^{-1}$ and -0.14 ‰ to -0.67 ‰, respectively and exhibit a significant covariation ($R^2 = 0.64$; $p\text{-value} < 0.05$). The relatively lower [Mo] is observed between ~ 30 and 14 ka cal BP ($0.29 \pm 0.12 \mu\text{g}\cdot\text{g}^{-1}$; 2SD; $n = 10$) compared to the period from ~ 14 ka cal BP to present ($0.62 \pm 0.35 \mu\text{g}\cdot\text{g}^{-1}$; 2SD; $n = 10$). The $\delta^{98}\text{Mo}$ shows the opposite trend, with $\delta^{98}\text{Mo}$ of -0.27 ± 0.20 ‰ (2SD; $n = 10$) from ~ 30 to 14 ka cal BP and $\delta^{98}\text{Mo}$ of

-0.50 ± 0.17 ‰ (2SD; $n = 10$) from ~ 14 ka cal BP to present.

5. Discussion

Mo concentrations of lake surface sediments are substantially higher compared to the bedrock concentrations ($0.022\text{--}0.58 \mu\text{g}\cdot\text{g}^{-1}$; Damanik et al., 2024). Although lacustrine [Mo] show an overlap with the catchment laterite substrates, most of the lake sediment samples show [Mo] values exceeding those in laterite samples ([Fig. 3a](#)). However, lake surface sediment and laterite profile samples show similar variations in Mo/Ti ratios ([Fig. 3b](#)). The average $\delta^{98}\text{Mo}$ composition of lake surface (-0.40 ‰; $n = 37$) and sediment core (-0.39 ‰; $n = 20$) are lower compared to that of the bedrock (-0.16 ‰; $n = 5$) and laterite samples (-0.2 ‰; $n = 17$), although a large overlap between lake sediments and laterite samples is observed ([Fig. 3a](#)). The covariation between [Mo] and distance from major river inlets ([Fig. 2a](#)) suggests physical processes such as transport and mineral sorting and dominant process for the Mo abundance variation within lake surface sediments. However, the overall lighter concentration-weighted Mo isotopic composition of lake surface sediments ($\delta^{98}\text{Mo} = -0.38$ ‰) compared to the catchment substrates ($\delta^{98}\text{Mo} = -0.05$) suggests that geochemical processes within the lake affect Mo mobility and its isotope composition in lake sediments.

5.1. Source, transport and sorting controls on [Mo] and $\delta^{98}\text{Mo}$ variability in Lake Towuti

The input of Mo into Lake Towuti is primarily governed by the erosion and transport of catchment bedrock and laterite substrates. During chemical weathering of the predominant ultramafic bedrock, Mo is residually enriched in the weathering product, with an enrichment factor (EF) of up to ~ 40 relative to its respective bedrock concentration (Damanik et al., 2024). This enrichment mainly occurs due to the adsorption of Mo during secondary mineral formation, particularly onto the ubiquitous Fe (oxyhydr)oxides, which form during chemical weathering as well as onto soil OM (Damanik et al., 2024). The effective retention of Mo released from bedrock during weathering results in a concentration-weighted average $\delta^{98}\text{Mo}$ composition of -0.05 ‰ ($n = 17$) in the laterite samples, which is within the 2SD analytical reproducibility, nearly identical to the bedrock $\delta^{98}\text{Mo}$ composition (-0.17 ‰; $n = 5$; [Fig. 3](#); Damanik et al., 2024). Substrates from the so-called weakly laterized zone, which represent the early stages of chemical weathering, are lower in [Mo] and have up to ~ 0.7 ‰ lower $\delta^{98}\text{Mo}$ compositions relative to the overlying more chemically evolved weathering substrates ([Fig. 3](#); Damanik et al., 2024).

Thus, differences in the type and style of erosion, such as surficial versus more deeply incised gully erosion (Hasberg et al., 2019), could explain some of the [Mo] and $\delta^{98}\text{Mo}$ variations we observe in lake sediments. The contrasting [Mo] between the bedrock and weakly laterized substrates and the more intensely weathered Fe (oxyhydr) oxide-rich substrates points to a key role of sediment sorting during transport in influencing [Mo] in the lake sediments. Hydrodynamic sorting effectively separates the finer-grained and low-density laterite substrates (Fe (oxyhydr)oxides and clay minerals) from the coarser, higher-density bedrock particles in Lake Towuti (Hasberg et al., 2019; Morlock et al., 2019; Sheppard et al., 2019). This process is best illustrated by the Al/Mg ratio of lake surface sediments ([Fig. S2](#); Morlock et al., 2019), where high values (more clay and less mafic minerals) indicate deposition of fine-grained, intensely weathered laterite substrates, and conversely, low values (less clay, more mafic/serpentine minerals) indicate the predominance of poorly weathered bedrock substrate deposition in higher energy environments close to river mouths. Low Al/Mg values are observed in lake surface sediments near major inlets, particularly around the Mahalona, Loeha and Lengke Rivers. In contrast, the highest Al/Mg values—and thus the predominance of fine-grained laterite substrates—are found in the deeper, more

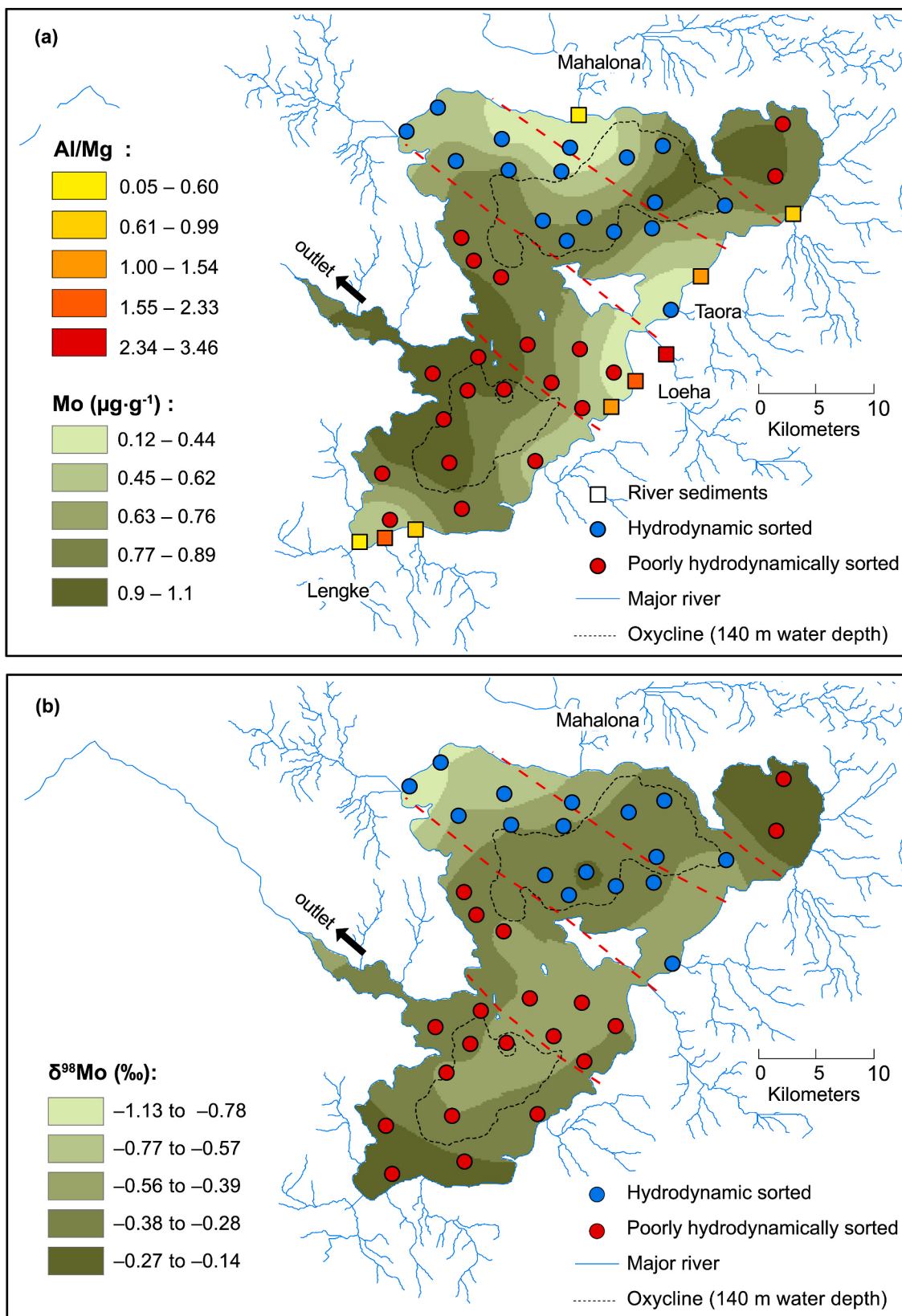


Fig. 2. (a) Mo concentration ($\mu\text{g}\cdot\text{g}^{-1}$) and $\delta^{98}\text{Mo}$ (%) in lake surface sediments. Blue circles represent predominantly fluvially transported, well-sorted ('hydrodynamically sorted') surface sediments from the northern basin. Red circles represent more poorly sorted ('poorly hydrodynamically sorted') surface sediments, transported over shorter distances from the northeastern and southern basins. Al/Mg values of river sediments in (a) originate from Morlock et al. (2019). (For interpretation of the references to color in this figure legend, the reader is referred to the Web version of this article.)

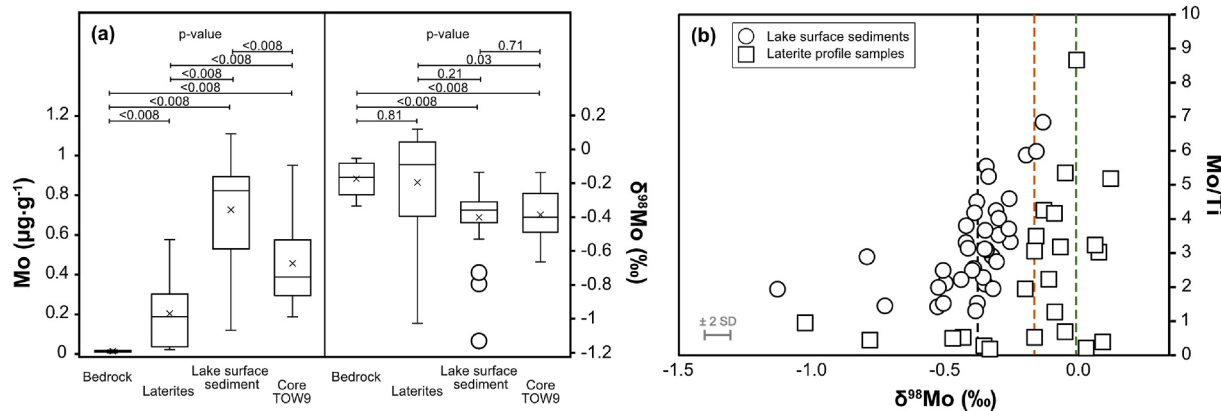


Fig. 3. (a) Boxplots of Mo concentration ($\mu\text{g}\cdot\text{g}^{-1}$) and $\delta^{98}\text{Mo}$ (‰) variability in Lake Towuti sediments and catchment bedrock and soil substrates. Data for the bedrock and laterites are available from Damanik et al. (2024), while lake surface sediments and TOW9 data are from this study. T-tests are performed for all 6 pairwise comparisons; therefore, the p-values are adjusted to the significance level to avoid false positives. (b) Mo/Ti ratio versus $\delta^{98}\text{Mo}$ (‰) of samples from the laterite profile and the lake surface sediments. The black dashed line is the concentration-weighted average $\delta^{98}\text{Mo}$ of lake surface sediments (-0.38‰; n = 37), green dashed line is the average of $\delta^{98}\text{Mo}$ values from peridotite bedrock (-0.17‰; n = 5; Damanik et al., 2024), and the orange dashed line is the concentration-weighted average $\delta^{98}\text{Mo}$ composition in the laterite samples overlying peridotite bedrock (-0.05‰; n = 17; Damanik et al., 2024). Error bars in (b) represent 2SD long-term external reproducibility.

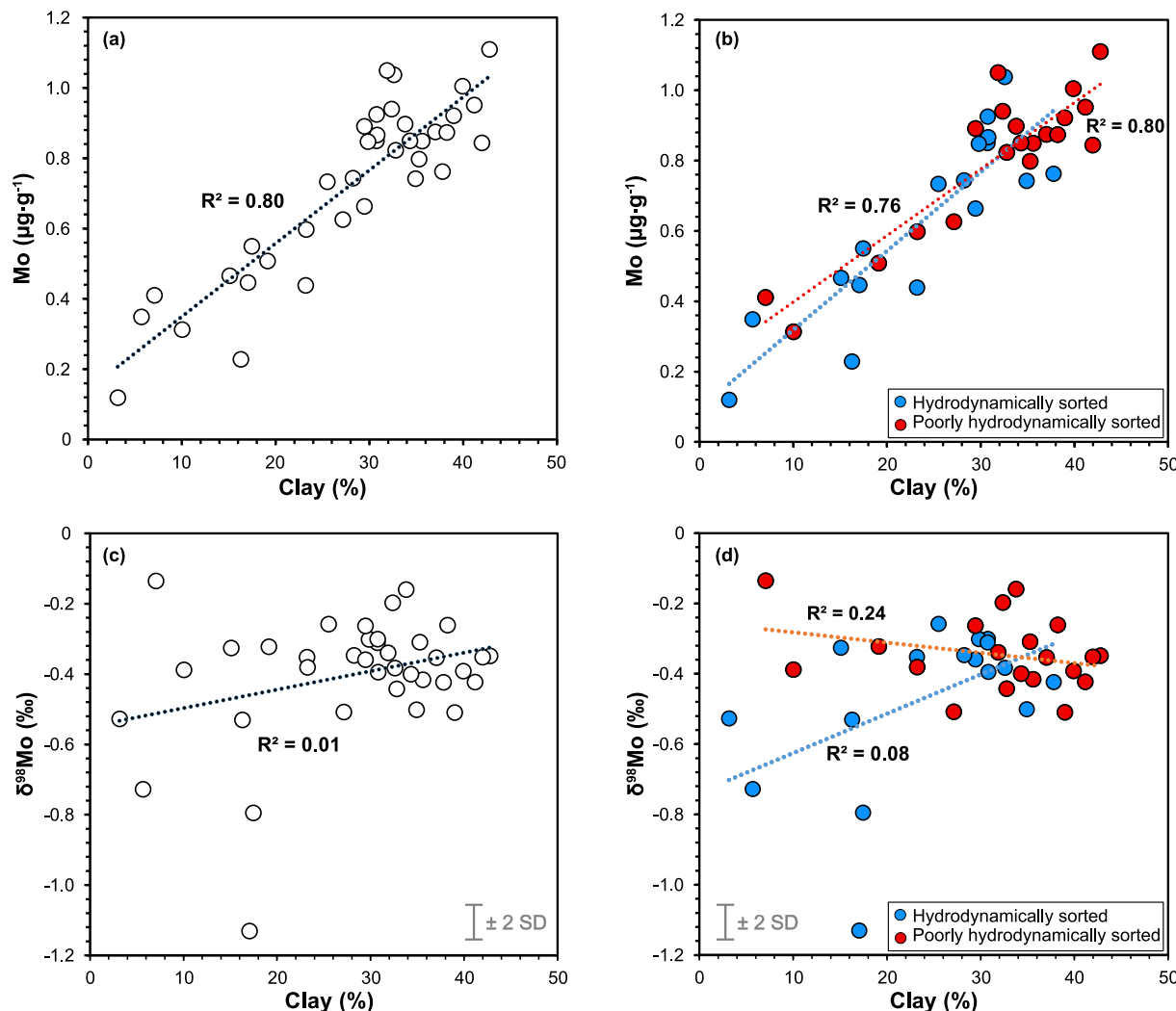


Fig. 4. Mo concentration ($\mu\text{g}\cdot\text{g}^{-1}$) versus (a) clay content (%) in all lake surface sediments, and (b) with separation between hydrodynamically sorted and poorly hydrodynamically sorted. $\delta^{98}\text{Mo}$ (‰) versus (c) clay content (%) in all lake surface sediments, and (d) with separation between hydrodynamically sorted and poorly hydrodynamically sorted. Error bars represent 2SD long-term external reproducibility.

distal parts of the larger basins A, B, C and D (Fig. S2; Hasberg et al., 2019; Sheppard et al., 2019). Similarly, clay content, which is lowest near the major inlets and highest in the most distal parts of the lake (Hasberg et al., 2019; Morlock et al., 2019), shows a positive correlation with [Mo] (Fig. 4a; $R^2 = 0.80$; p-value < 0.05 for all samples; Fig. 4b; $R^2 = 0.76$; p-value < 0.05 for hydrodynamically sorted samples; $R^2 = 0.80$; p-value < 0.05 for poorly hydrodynamically sorted samples). The effect of hydrodynamic sorting is most evident in the distribution of [Mo], with lower [Mo] near the Mahalona, Loeha and Lengke River mouths, and increasing concentrations towards the centers of basins A, B, C and D (Fig. 2a). This pattern is partly explained by lower [Mo] in the coarse-grained, bedrock-dominated sediments compared to the finer-grained lateritic substrates (Damanik et al., 2024). While this correlation is consistent with hydrodynamic sorting concentrating fine particles in distal, low-energy depositional environments, we note that clay-rich sediments in Lake Towuti are also frequently associated with elevated OM content (Hasberg et al., 2019), which can enhance trace metal retention. Moreover, the deposition distal to the major inlets often coincides with deeper anoxic water, reflecting the tendency for hydrodynamic sorting to concentrate fine-grained, OM-rich sediments (Hasberg et al., 2019) in settings that also favor Mo enrichment. Therefore, while hydrodynamic sorting is the primary process controlling [Mo] in Lake Towuti, the associated accumulation of OM and the prevalence of anoxic conditions further amplify Mo enrichment.

In smaller basin E, hydrodynamic sorting seems less prominent, likely due to reduced runoff from smaller catchments and rivers, limited transport distance, and steeper slope gradients. In addition, these settings in Lake Towuti also receive sediments from frequent mass wasting, which often mobilizes the entire laterite weathering profiles (Morlock et al., 2019). Steep slopes have been shown to contain high clay-sized substrates (Hasberg et al., 2019), which are often associated with elevated OM content, potentially resulting in localized [Mo] enrichment in proximity to steeper catchment slopes. Similarly to basin E, the western shoreline of basins C and D is affected more frequently by mass-wasting (Tournier et al., 2023), which likely contributes to the homogenization of transported bedrock and laterite substrates (Morlock et al., 2019). These processes likely contribute to explaining the observed contrast between higher [Mo] proximal to the steeper catchment slopes and lower [Mo] and $\delta^{98}\text{Mo}$ in the deeper parts of these basins (Fig. 2). This mechanism also contributes to explaining the strong [Mo]-clay relationship even in settings where hydrodynamic sorting is less prevalent and direct slope to basin transfer is predominant (Fig. 4b).

Given the low [Mo] in the weakly laterized zone and the limited volume it occupies within the weathering profile, it is unlikely that variations in the style of erosion alone exert an appreciable impact on the Mo isotope composition of Lake Towuti's sediments. Therefore, the input of isotopically light Mo from weakly laterized catchment substrates with a low $\delta^{98}\text{Mo}$ is unable to explain the overall lighter Mo isotope composition of lake sediments. Moreover, in contrary to the [Mo] distribution pattern in Lake Towuti, surface sediments $\delta^{98}\text{Mo}$ and grain-size data show absence of a significant correlation (Fig. 4c; $R^2 = 0.1$; p-value < 0.05 for all samples; Fig. 4d; $R^2 = 0.24$; p-value < 0.05 for hydrodynamically sorted samples; $R^2 = 0.08$; p-value < 0.2 for poorly hydrodynamically sorted samples). This suggests that mineral sorting is unlikely to play a substantial control in sedimentary $\delta^{98}\text{Mo}$. However, clay content in Lake Towuti reflects hydrodynamic sorting of distinct mineral phases: coarser-grained nearshore sediments are enriched in largely unweathered bedrock minerals, whereas fine-grained distal sediments are enriched in laterite-derived minerals like Fe (oxyhydr) oxides and clays (Hasberg et al., 2019). While $\delta^{98}\text{Mo}$ values of bedrock and highly weathered laterite substrates are largely similar, individual mineral hosts within these substrates can have distinct $\delta^{98}\text{Mo}$ signatures. A recent study by Wang et al. (2020) showed that Fe-Mn hydroxides tend to host heavier Mo isotopes, while residual Fe-Ti oxides exhibit lighter Mo isotope signatures. These minerals coexist within the same lateritic profiles and differ in density, making them susceptible to hydrodynamic

sorting. In our dataset, taking all lake surface sediments into account, a much lighter concentration-weighted $\delta^{98}\text{Mo}$ compared to the lateritic source (Fig. 3), with three samples exhibiting a very light Mo isotope composition close to river mouths (Fig. 2b), are observed. We applied the endmember $\delta^{98}\text{Mo}$ value of -1.13‰ and a Mo concentration of $1.0 \mu\text{g}\cdot\text{g}^{-1}$ to estimate whether enrichment in dense, Ti-rich mineral phases could explain these values. However, our calculations suggest that Ti concentrations in the sediment would need to be up to six times higher than what is actually measured to account for this shift. Thus, while hydrodynamic sorting and associated mineral-phase separation may contribute to some local $\delta^{98}\text{Mo}$ variations, especially near inflows, the consistently light $\delta^{98}\text{Mo}$ across the lake likely reflects an additional Mo mobilization or fractionation process beyond simple mineral sorting.

5.2. Redox controls on [Mo] and $\delta^{98}\text{Mo}$ variability in Lake Towuti

The Fe mineralogy in Lake Towuti varies from source to sink due to geochemical cycling among different mineral hosts, with the crystalline Fe, such as goethite and hematite, being more abundant in the laterite samples than in the lake surface sediment samples (Sheppard et al., 2019). These Fe-rich laterite substrates enter the lake and undergo reductive dissolution at and below the oxycline as well as in the sediments during early diagenesis just below the sediment-water interface (Bauer et al., 2020; Friese et al., 2021; Vuillemin et al., 2016). During reductive dissolution of Fe oxides, adsorbed metals can be released into the water column, a process observed in both ferruginous and euxinic environments (Algeo and Lyons, 2006; Crowe et al., 2008; Janssen et al., 2024). Based on previous work showing near-complete scavenging of Mo by Fe (oxyhydr)oxides in the catchment laterite weathering profiles of Lake Towuti (Damanik et al., 2024), we infer that Mo is remobilized during reductive dissolution of Fe oxides in the anoxic water column and surface sediments. Dissolved Fe^{2+} from either pore water or the anoxic water column migrates upwards to the oxycline, where it is ultimately reoxidized forming amorphous endogenic Fe oxides as documented in nearby Lake Matano with a similar water column structure and chemistry (Crowe et al., 2008). A downcore increase in Fe^{2+} concentrations in pore water of sediment cores taken from shallow oxic to deep anoxic water in Lake Towuti (Vuillemin et al., 2016) supports the idea of Fe^{3+} reduction just below the sediment-water interface. As a consequence, the ratio of crystalline iron to newly formed amorphous iron in lake surface sediment is lower compared to the lateritic source (Sheppard et al., 2019), suggesting active Fe cycling within lake sediments. In sediments deposited in oxic bottom waters, the newly amorphous Fe oxides are formed at the sediment-water interface sourced from the oxygenation of Fe^{2+} liberated from pore water. This likely leads to adsorption of the isotopically light Mo, with partial deposition and preservation of these authigenic precipitates above the oxycline in Lake Towuti. This explains the presence of lower $\delta^{98}\text{Mo}$ in surface sediments above the oxycline compared to those in laterite substrates (Figs. 2b and 3). This mechanism aligns with findings demonstrating that light Mo isotopes are preferentially adsorbed onto Fe oxides in batch experiments (Barling and Anbar, 2004; Goldberg et al., 1996, 2009) and in the lacustrine setting (Malinovsky et al., 2007). Therefore, we propose that active redox cycling of Fe and Mo significantly contributes to the observed spatial distribution of $\delta^{98}\text{Mo}$ in surface sediments.

Sheppard et al. (2019) noted the absence of a clear correlation between the abundance of crystalline and amorphous iron oxides in surface sediments and water depth, possibly due to the kinetics of Fe dissolution, combined with periodic water column mixing, which can obscure this relationship. This could explain the weak covariation between $\delta^{98}\text{Mo}$ vs. water depth in Towuti's surface sediments ($R^2 = 0.24$; p-value < 0.05; Fig. 5a). However, a strong correlation between $\delta^{98}\text{Mo}$ vs. water depth is observed in the larger northern basins A and B with a cumulative R^2 of 0.72 (p-value < 0.05; Fig. 5b). The $\delta^{98}\text{Mo}$ data reveal a distinct separation: a large range of low $\delta^{98}\text{Mo}$ values in the oxic waters (-1.13‰ to -0.35‰) and a smaller range of higher $\delta^{98}\text{Mo}$ values in the

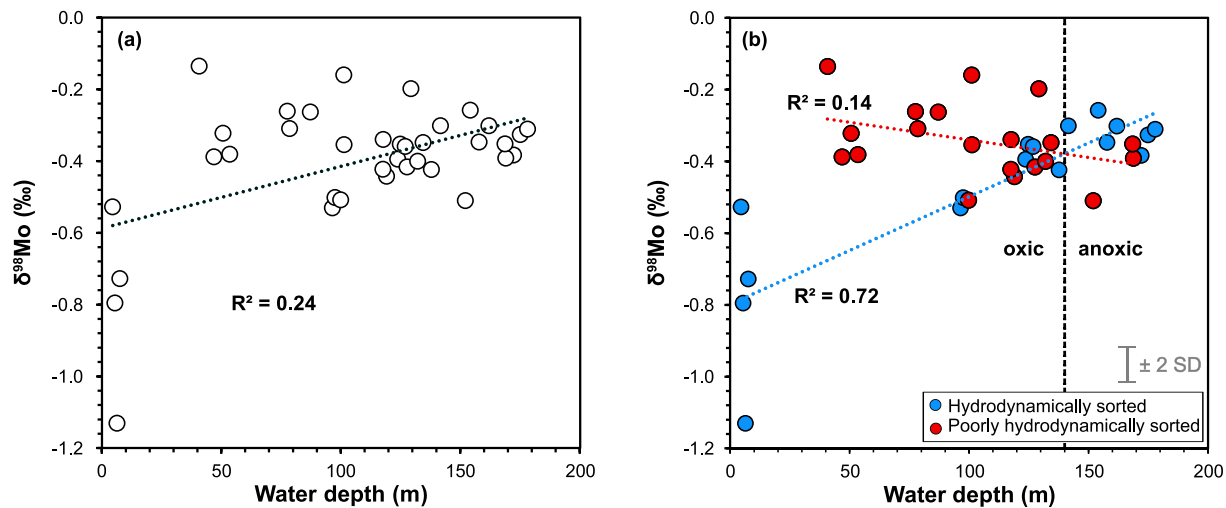


Fig. 5. $\delta^{98}\text{Mo}$ (‰) versus (a) water depth (m) in all lake surface sediments, and (b) with separation between hydrodynamically sorted and poorly hydrodynamically sorted. Error bars represent 2SD long-term external reproducibility.

anoxic waters (-0.38 ‰ to -0.26 ‰), closely aligning the modern oxycline at $\sim 140\text{ m}$ water depth (Fig. 5b; Costa et al., 2015). In contrast, samples from Basins C, D, and E, show a weaker correlation likely due to low slope stability and more frequent mass movements, which homogenize the Mo isotope signals and potentially obscure Fe mineralogical signals as well (Fig. 5b). These findings suggest that stable, longer-distance transport, with less mass wasting and periodic water column mixing, may be necessary to facilitate stable Fe redox cycling and enhance the distinctive Mo isotope signature in the sediments.

Furthermore, the adsorption of isotopically light Mo results in isotopically heavy dissolved Mo in the water column. This heavy Mo subsequently can adsorb onto OM, especially in the deep anoxic part of Lake Towuti (Fig. 6) where the preservation of OM is enhanced. This may partially explain the higher $\delta^{98}\text{Mo}$ in the deeper anoxic water column with higher OM content (Fig. 6b). Samples near the Mahalona River mouth (Surf9 and Surf16) deviate from this trend, with low [Mo] and high TOC, suggesting additional factors, such as the availability of dissolved Mo and/or the type of OM. Higher OM in close proximity to the Mahalona River mouth is largely related to the deposition of terrestrial OM in the form of plant fragments (Vogel et al., 2015) indicated by enriched $\delta^{13}\text{C}$ in this area (Hasberg et al., 2019). In these nearshore

environments, it is also expected that only small amounts of Mo in solution are available for scavenging by OM. Excluding these samples, we find a significant correlation between [TOC] and [Mo] ($R^2 = 0.83$; p-value < 0.05; Fig. 6a), with higher [TOC] in the anoxic part of the lake corresponding to higher [Mo] and high $\delta^{98}\text{Mo}$ (Fig. 6b). This relationship between [Mo] and [TOC] has been used to interpret past redox conditions in marine environments, where Mo enrichment in sediments is associated with anoxic conditions, in which high OM content and effective OM scavenging enhance Mo accumulation (Algeo and Lyons, 2006; Tribouillard et al., 2006).

The limited correlation between sedimentary $\delta^{98}\text{Mo}$ and [TOC], but rather a separation of isotopically heavier Mo with higher OM content (Fig. 6b), suggests that Mo scavenging in Lake Towuti is predominantly controlled by OM in the deeper anoxic parts and by Fe oxyhydroxides in the shallower oxic parts of the water column. Sheppard et al. (2019) suggest that the abundance of crystalline iron phases is relatively homogeneously distributed across the lake, possibly due to biologically mediated Fe cycling processes and frequent water column mixing. Nevertheless, the preferential scavenging of isotopically light Mo onto newly formed amorphous Fe oxides results in Mo isotope fractionation with isotopically heavy Mo reservoirs in Lake Towuti's water column.

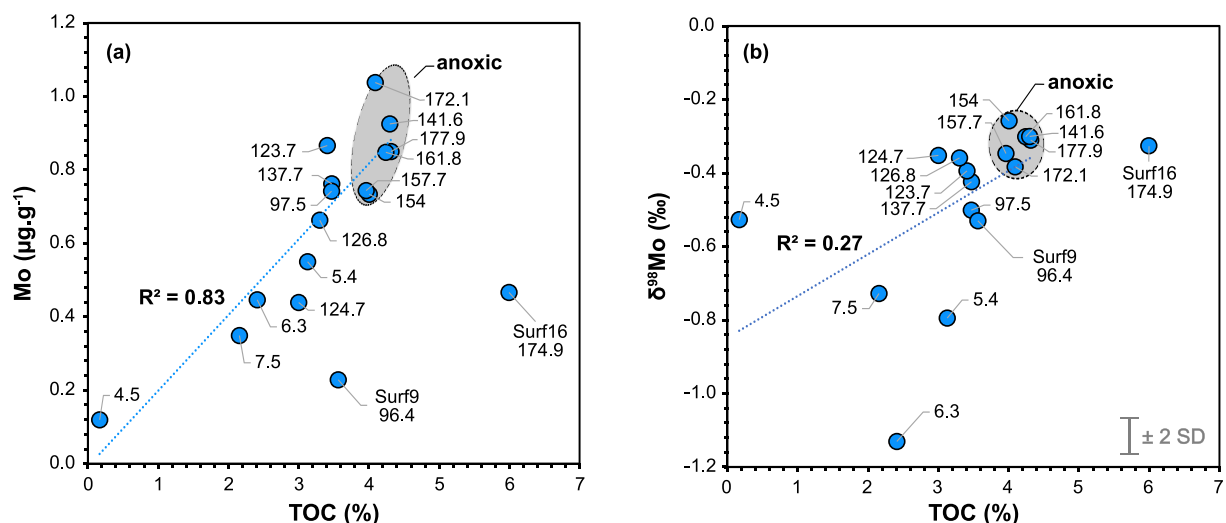


Fig. 6. (a) Mo concentration ($\mu\text{g}\cdot\text{g}^{-1}$) and (b) $\delta^{98}\text{Mo}$ (‰) versus TOC (%) in hydrodynamically sorted lake surface sediments. The labels indicate the respective water depth in meters below the lake surface of the sampling location. Error bars represent 2SD long-term external reproducibility.

The better preservation of OM below the oxycline (Hasberg et al., 2019; Vuillemin et al., 2016) effectively removes dissolved Mo and contributes to the higher $\delta^{98}\text{Mo}$ values in the anoxic sediments compared to those deposited in oxic waters (Fig. 6b). This highlights the importance of OM flux and preservation on Mo cycling in stratified and anoxic lake basins.

Importantly, Fe redox cycling and the dominant role of OM in governing Mo isotope cycling in ferruginous settings represents a key distinction from the well-established Mo removal via thiomolybdate formation in euxinic environments (Algeo and Lyons, 2006; Nägler et al., 2011). This highlights that the Mo isotope signature in this lacustrine endmember may not reflect simple quantitative removal of dissolved Mo, but instead results from dynamic interactions of Fe oxides phases and OM. Nonetheless, the distinctive $\delta^{98}\text{Mo}$ signatures between sediments deposited in oxic versus anoxic parts of today's water column underscore the potential use of Mo as a proxy for water column oxygenation over a longer time scale.

5.3. Molybdenum variability as a water column (de-)oxygenation proxy over the past ~30 ka in Lake Towuti

The observed spatial variability in [Mo] and $\delta^{98}\text{Mo}$ in Towuti's modern surface sediments form a valuable basis to understand hydrodynamic sorting and redox relationships in sediment records. Indeed, downcore [Mo] and $\delta^{98}\text{Mo}$ variability in core TOW9 shows a range in values comparable to that observed in modern lake surface sediments (Figs. 4 and 7a, b). The downcore trends in [Mo] and $\delta^{98}\text{Mo}$ align with climate proxies and climate-sensitive indicators for erosion, transport, vegetation structure, depositional processes, and redox conditions in core TOW9 (Fig. 7). Lower [Mo] during the last glacial maximum between ~30 and 14 ka cal BP is in part interpreted to reflect less efficient hydrodynamic sorting due to lower lake levels and shorter transport distances between the inlets and the coring site (Fig. 7h; Vogel et al., 2015). Less efficient hydrodynamic sorting results in the deposition of coarser-grained and Mo-depleted bedrock substrates at site TOW9 (Fig. 7c). Previous studies on core TOW9 (Morlock et al., 2019) also reported coarser sediments with higher proportions of less weathered bedrock substrates during the last glacial maximum. The correlation of low $\delta^{98}\text{Mo}$ with low [Mo] in sediments deposited during the last glacial closely mirrors the signatures found in the shallow, oxic part of the lake today, where [TOC] is low due to effective remineralization (Fig. 7). Low [TOC], reddish sediment colors and high concentrations of reactive and total Fe species (Russell et al., 2020; Sheppard et al., 2019) are likewise reported for sediments deposited during the last glacial maximum in Lake Towuti suggesting complete mixing and deep water oxygenation thereby strongly supporting our interpretation of Mo signatures being indicative for water column oxygenation down to the sediment-water interface. Deep mixing and full water column oxygenation are the results of a slightly colder water column and reduced downwelling long-wave radiation (Fig. 7i; Parish et al., 2023) and substantially drier (Konecky et al., 2016; Russell et al., 2014; Vogel et al., 2015; Wicaksono et al., 2015) climate conditions with more evaporative cooling of surface waters and associated mixing of the water column during the last glacial period (Fig. 7; Costa et al., 2015; Russell et al., 2014, 2020).

In contrast, high [Mo] and $\delta^{98}\text{Mo}$ in sediments deposited during the Holocene align with sedimentary indicators of permanent stratification, including a green sediment color, generally lower reactive and total Fe species concentrations, and higher [TOC] (Fig. 7d, e, f). As a result, the period between ~14 ka and the present is marked by quasi-permanent stratification, with anoxic bottom water in warm and wet interglacial climate conditions and lake levels similar to those of today (Fig. 7; Costa et al., 2015; Russell et al., 2014, 2020; Vogel et al., 2015). The observed high [Mo] and $\delta^{98}\text{Mo}$ values are the result of a warmer water column and permanent stratification and bottom water anoxia as well as a more effective hydrodynamic sorting similar to today.

The shift toward permanent stratification, as indicated by higher

$\delta^{98}\text{Mo}$ starting at ~14 cal ka BP, aligns with the synthesized changepoint of precipitation for the Indo-Pacific Warm Pool, which various records place at ~12.3 cal ka BP (black dashed line in Fig. 7; Parish et al., 2024). This significant increase in precipitation and humidity reduces the effect of evaporative cooling and thereby water column mixing in Lake Towuti (Costa et al., 2015). Additionally, the ~3 °C increase in temperature from the last glacial maximum to the Holocene is consistent with other regional reconstructions (Parish et al., 2023, 2024; Zhao et al., 2023) and contributes to the stability of the stratification. The gradual increase in [Mo] is closely associated with the gradual increase of TOC coinciding with the transition to a closed-canopy forest (Russell et al., 2014; green dashed line in Fig. 7; Parish et al., 2024) with a notable increase at ~14 cal ka BP. This suggests that the observed beginning of the increase in Mo could be additionally driven by a higher catchment to lake nutrient and OM flux alongside better preservation of OM in anoxic bottom water resulting in more efficient adsorption and deposition of Mo during this transition (Fig. 6a).

The consistent relationship between [Mo], $\delta^{98}\text{Mo}$, and climate-driven water column oxygenation indicates that Mo can serve as a reliable proxy of past water column (de)oxygenation. Post-depositional remobilization of Mo was not observed and is assumed to be of minor influence. Consequently, Mo elemental and isotope signatures in sediment records are effective tools for reconstructing past water column oxygenation and hydrodynamic regimes in modern and ancient aquatic environments.

6. Conclusion

The analysis of [Mo] and $\delta^{98}\text{Mo}$ in Lake Towuti's surface sediments reveals that Mo concentration is primarily controlled by hydrodynamic sorting and OM preservation, while Mo isotope fractionation is largely controlled by water column oxygenation. In basins with effective hydrodynamic sorting and sufficient transport distances, [Mo] is enriched in the fine fraction. Active redox cycling of Fe plays a key role in controlling $\delta^{98}\text{Mo}$. Reductive dissolution of Fe (oxyhydr)oxides in anoxic bottom waters and sediments releases Mo, which is then scavenged by reprecipitated newly formed amorphous Fe oxides in the oxic parts of the water column and sediments. The data from Lake Towuti suggests that the active redox cycling of Fe and Mo leads to isotope fractionation of Mo resulting in lighter $\delta^{98}\text{Mo}$ signatures of sediments deposited in the oxic part of the water column. Consequently, this process drives the remaining reservoir towards heavy Mo isotope compositions. High $\delta^{98}\text{Mo}$ signatures are indicative of sediments deposited in anoxic parts of the water column and closely associated with high OM contents suggesting that heavy $\delta^{98}\text{Mo}$ accumulating in the water column is removed and deposited through scavenging by OM.

These patterns of Mo isotope fractionation linked to water column oxygenation are also preserved in deeper sediments, spanning the last glacial maximum through the Holocene period. During the cold and dry glacial period, low $\delta^{98}\text{Mo}$ values correspond to conditions of regular mixing and full oxygenation of the water column. In contrast, high $\delta^{98}\text{Mo}$ values in Holocene sediments reflect a warm and wet climate that promoted permanent water column stratification and persistently anoxic bottom waters. The overall $\delta^{98}\text{Mo}$ variability in these sediments effectively records water column oxygenation, largely unaffected by post-depositional processes, making it a reliable proxy for modern and past water column oxygenation in Lake Towuti and similar aquatic depositional environments.

Beyond its relevance for Mo behaviour in modern lacustrine settings, our study provides important implications for the reconstruction of global marine Mo mass balance under ferruginous conditions in Earth's early oceans (Planavsky et al., 2011; Poulton and Canfield, 2011; Scott et al., 2008). Quantitative removal of isotopically light Mo in form of MoO_4^{2-} adsorption onto Mn-oxide-rich pelagic sediments, representing 30 % of the global ocean Mo output today (Kendall et al., 2017), was likely absent in early oceans. Instead, shuttling of Mn and Fe oxides at

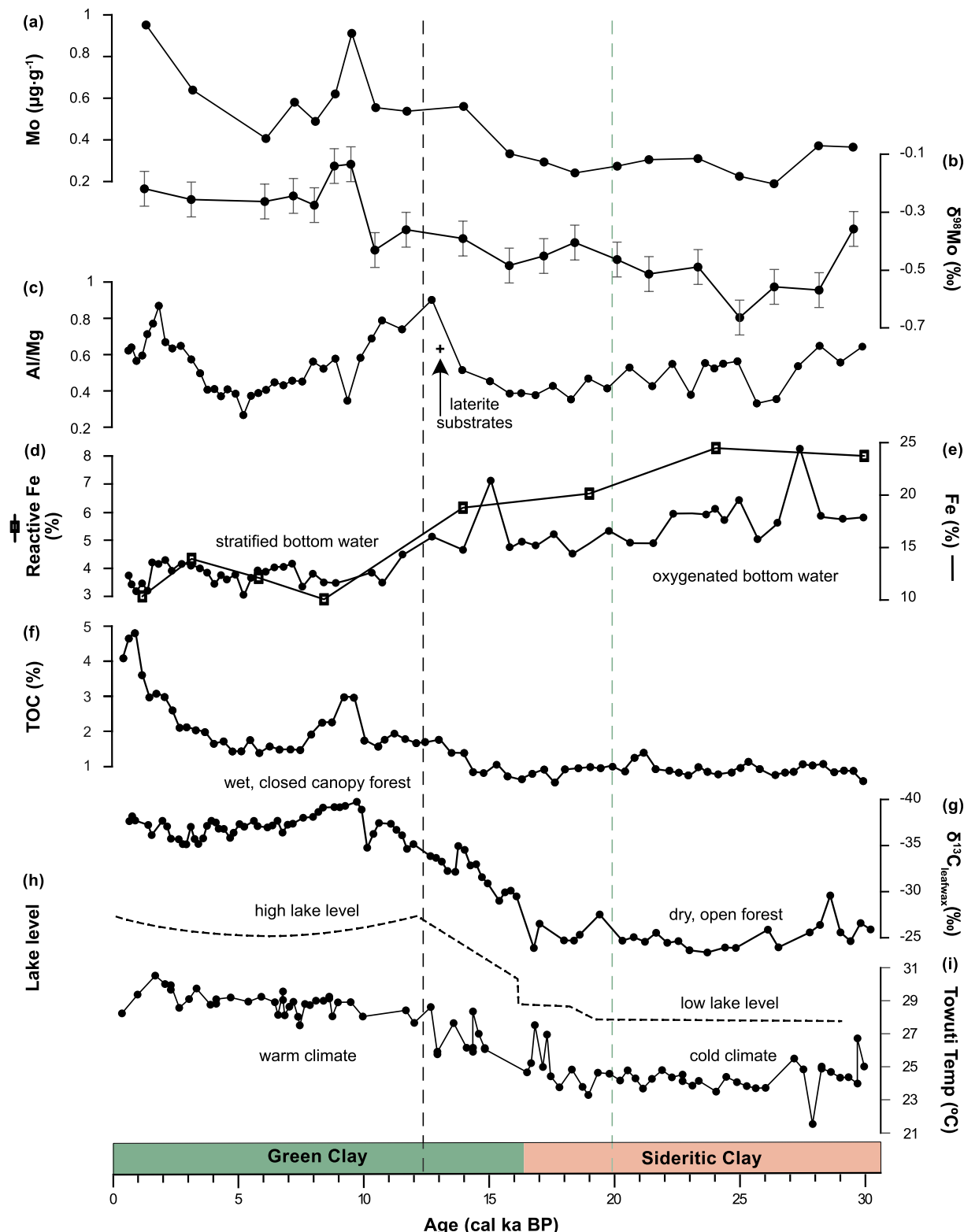


Fig. 7. (a) Mo concentration ($\mu\text{g}\cdot\text{g}^{-1}$) and (b) $\delta^{98}\text{Mo} (\text{\textperthousand})$ from core TOW 9 plotted on an age-scale, along with various proxies obtained from the same sediment core: (c) Al/Mg as a source proxy, (d) reactive Fe (%) and (e) Fe (%) as redox proxies (Russell et al., 2020; Sheppard et al., 2019), (f) TOC (wt%) as an organic input proxy (Russell et al., 2020), (g) $\delta^{13}\text{C}_{\text{leafwax}} (\text{\textperthousand})$ as a climate proxy (Russell et al., 2014), (h) tentative lake-level reconstruction for Lake Towuti (Vogel et al., 2015), (i) Temperature reconstructed from brGDGT from Lake Towuti (Parish et al., 2023, 2024; Zhao et al., 2023). The black vertical dashed line indicates the changepoint of precipitation at ~ 12.3 cal ka BP in the Indo-Pacific Warm Pool (Parish et al., 2024), while the green dashed line indicates the vegetation shift at ~ 19.9 cal ka BP due to the seasonality in precipitation (Parish et al., 2024). (For interpretation of the references to color in this figure legend, the reader is referred to the Web version of this article.)

water column redox interfaces along continental margins (Ossa et al., 2018; Planavsky et al., 2014) may have had a much larger impact on the global Mo cycle compared to modern oceans. At these redox interfaces, the formation of oxides and the adsorption of dissolved Mo likely enhanced the flux of isotopically light Mo to sediments, while early diagenetic porewater redox changes and fluctuating bottom-water oxygenation further fractionated Mo isotopes and yielded sediments with low $\delta^{98}\text{Mo}$. Likely these continental margin settings have acted as a more significant sink of isotopically light Mo from the early oceans compared to modern open-marine anoxic margin settings (Scholz et al., 2017).

Our findings from Lake Towuti demonstrate that, under ferruginous conditions, Mo isotope signatures are not solely governed by quantitative Mo uptake from seawater, as in sulfidic settings, but instead by dynamic cycling between Fe(oxyhydr)oxides and OM, leading to sediment $\delta^{98}\text{Mo}$ ratios closer to that of contemporaneous seawater. This reinforces the need to interpret ancient $\delta^{98}\text{Mo}$ records in the context of both redox conditions and depositional environment. Therefore, further investigation of Mo cycling in ferruginous lake settings can serve as valuable modern analogs for testing Mo cycling hypotheses and Mo isotope systematics during the transition from ferruginous to euxinic ocean conditions. Moreover, in situ water column measurements of Mo and related redox-sensitive elements, particularly across the oxycline, would help refine our understanding of Fe–Mo cycling and isotope fractionation mechanisms in ferruginous water columns and should be a priority for future studies.

Author contributions

Adrianus Damanik: Writing – review & editing, Writing – original draft, Visualization, Methodology, Investigation, Formal analysis, Data curation. Martin Wille: Writing – review & editing, Visualization, Supervision, Methodology, Formal analysis, Data curation, Conceptualization. Qasid Ahmad: Writing – review & editing, Methodology, Data curation. Sean A. Crowe: Writing – review & editing. Koen W. Bauer: Writing – review & editing. Martin Grosjean: Writing – review & editing, Supervision. Sri Yudawati Cahyarini: Writing – review & editing, Supervision, Funding acquisition. Satria Bijaksana: Writing – review & editing. James M. Russell: Writing – review & editing, Funding acquisition. Hendrik Vogel: Writing – review & editing, Writing – original draft, Supervision, Resources, Project administration, Investigation, Funding acquisition, Conceptualization.

Declaration of competing interest

The authors declare that they have no known competing financial interests or personal relationships that could have appeared to influence the work reported in this paper.

Acknowledgements

This research was carried out with support from the German Research Foundation (DFG) and the Swiss National Science Foundation (SNSF) through grants awarded to H. Vogel (DFG: VO 1591/2-1; SNSF: 200020_188876 & 200021_153053) as well as through the U.S. National Science Foundation (NSF) through grants awarded to J.M. Russell. Foreign research permits for field work at Lake Towuti were kindly granted by the Ministry of Research, Education, and Higher Technology of Indonesia (RISTEK) permit number 02/TKPIPA/FRP/SM/II/2010. Logistical support was kindly provided by PT Vale Indonesia. We also thank two anonymous reviewers for their constructive reviews, as well as Mira Matthews for editorial handling.

Appendix A. Supplementary data

Supplementary data to this article can be found online at <https://doi.org/10.1016/j.quascirev.2025.109607>.

<https://doi.org/10.1016/j.quascirev.2025.109607>.

Data availability

All data and/or code is contained within the submission.

References

- Ahmad, Q., Wille, M., König, S., Rosca, C., Hensel, A., Pettke, T., Hermann, J., 2021. The Molybdenum isotope subduction recycling conundrum: a case study from the Tongan subduction zone, Western Alps and Alpine Corsica. *Chem. Geol.* 576, 120231. <https://doi.org/10.1016/j.chemgeo.2021.120231>.
- Ahmad, Q., Wille, M., Labidi, J., König, S., Devey, C., Mezger, K., 2023. Heavy Mo isotope enrichment in the Pitcairn plume: implications for the subduction cycle of anoxic sediments. *Earth Planet Sci. Lett.* 624, 118466. <https://doi.org/10.1016/j.epsl.2023.118466>.
- Ahmad, Q., Wille, M., Rosca, C., Labidi, J., Schmid, T., Mezger, K., König, S., 2022. Molybdenum isotopes in plume-influenced MORBs reveal recycling of ancient anoxic sediments. *Geochem. Perspect. Lett.* 23, 43–48. <https://doi.org/10.7185/geochemlett.2236>.
- Algeo, T.J., Lyons, T.W., 2006. Mo-total organic carbon covariation in modern anoxic marine environments: implications for analysis of paleoredox and paleohydrographic conditions. *Paleoceanography* 21, 2004PA001112. <https://doi.org/10.1029/2004PA001112>.
- Arnold, G.L., Anbar, A.D., Barling, J., Lyons, T.W., 2004. Molybdenum isotope evidence for widespread anoxia in mid-proterozoic oceans. *Science* 304, 87–90. <https://doi.org/10.1126/science.1091785>.
- Barling, J., Arnbar, A.D., 2004. Molybdenum isotope fractionation during adsorption by manganese oxides. *Earth Planet Sci. Lett.* 217, 315–329. [https://doi.org/10.1016/S0012-821X\(03\)00608-3](https://doi.org/10.1016/S0012-821X(03)00608-3).
- Barling, J., Arnold, G.L., Anbar, A.D., 2001. Natural mass-dependent variations in the isotopic composition of molybdenum. *Earth Planet Sci. Lett.* 193, 447–457. [https://doi.org/10.1016/S0012-821X\(01\)00514-3](https://doi.org/10.1016/S0012-821X(01)00514-3).
- Bauer, K.W., Byrne, J.M., Kenward, P., Simister, R.L., Michiels, C.C., Friese, A., Vuillemin, A., Henny, C., Nomosatryo, S., Kallmeyer, J., Kappler, A., Smit, M.A., Francois, R., Crowe, S.A., 2020. Magnetite biomineralization in ferruginous waters and early Earth evolution. *Earth Planet Sci. Lett.* 549, 116495. <https://doi.org/10.1016/j.epsl.2020.116495>.
- Bauer, K.W., Gueguen, B., Cole, D.B., Francois, R., Kallmeyer, J., Planavsky, N., Crowe, S.A., 2018. Chromium isotope fractionation in ferruginous sediments. *Geochim. Cosmochim. Acta* 223, 198–215. <https://doi.org/10.1016/j.gca.2017.10.034>.
- Bertine, K.K., Turekian, K.K., 1973. Molybdenum in marine deposits. *Geochim. Cosmochim. Acta* 37, 1415–1434. [https://doi.org/10.1016/0016-7037\(73\)90080-X](https://doi.org/10.1016/0016-7037(73)90080-X).
- Boehr, B., Schultz, M., 2008. Stratification of lakes. *Rev. Geophys.* 46, 2006RG000210. <https://doi.org/10.1029/2006RG000210>.
- Brown, E.T., Le Callonnec, L., German, C.R., 2000. Geochemical cycling of redox-sensitive metals in sediments from lake Malawi: a diagnostic paleotracer for episodic changes in mixing depth. *Geochim. Cosmochim. Acta* 64, 3515–3523. [https://doi.org/10.1016/S0016-7037\(00\)00460-9](https://doi.org/10.1016/S0016-7037(00)00460-9).
- Brucker, R.L.P., McManus, J., Severmann, S., Berelson, W.M., 2009. Molybdenum behavior during early diagenesis: insights from Mo isotopes. *G-cubed* 10, 2008GC002180. <https://doi.org/10.1029/2008GC002180>.
- Busigny, V., Planavsky, N.J., Jézéquel, D., Crowe, S., Louvat, P., Moureau, J., Viollier, E., Lyons, T.W., 2014. Iron isotopes in an Archean ocean analogue. *Geochim. Cosmochim. Acta* 133, 443–462. <https://doi.org/10.1016/j.gca.2014.03.004>.
- Canfield, D.E., Thamdrup, B., Hansen, J.W., 1993. The anaerobic degradation of organic matter in Danish coastal sediments: iron reduction, manganese reduction, and sulfate reduction. *Geochim. Cosmochim. Acta* 57, 3867–3883. [https://doi.org/10.1016/0016-7037\(93\)90340-3](https://doi.org/10.1016/0016-7037(93)90340-3).
- Cannon, D.J., Troy, C., Bootsma, H., Liao, Q., MacLellan-Hurd, R., 2021. Characterizing the seasonal variability of hypolimnetic mixing in a large, deep lake. *J. Geophys. Res. Oceans* 126, e2021JC017533. <https://doi.org/10.1029/2021JC017533>.
- Chappaz, A., Lyons, T.W., Gordon, G.W., Anbar, A.D., 2012. Isotopic fingerprints of anthropogenic molybdenum in lake sediments. *Environ. Sci. Technol.* 46, 10934–10940. <https://doi.org/10.1021/es3019379>.
- Costa, K.M., Russell, J.M., Vogel, H., Bijaksana, S., 2015. Hydrological connectivity and mixing of Lake Towuti, Indonesia in response to paleoclimatic changes over the last 60,000 years. *Palaeogeogr. Palaeoclimatol. Palaeoecol.* 417, 467–475. <https://doi.org/10.1016/j.palaeo.2014.10.009>.
- Crowe, S.A., O'Neill, A.H., Katsev, S., Hehanussa, P., Haffner, G.D., Sundby, B., Mucci, A., Fowle, D.A., 2008. The biogeochemistry of tropical lakes: a case study from Lake Matano, Indonesia. *Limnol. Oceanogr.* 53, 319–331. <https://doi.org/10.4319/lo.2008.53.1.0319>.
- Dahl, T.W., Anbar, A.D., Gordon, G.W., Rosing, M.T., Frei, R., Canfield, D.E., 2010. The behavior of molybdenum and its isotopes across the chemocline and in the sediments of sulfidic Lake Cadagno, Switzerland. *Geochim. Cosmochim. Acta* 74, 144–163. <https://doi.org/10.1016/j.gca.2009.09.018>.
- Dahl, T.W., Chappaz, A., Fitts, J.P., Lyons, T.W., 2013. Molybdenum reduction in a sulfidic lake: evidence from X-ray absorption fine-structure spectroscopy and implications for the Mo paleoproxy. *Geochim. Cosmochim. Acta* 103, 213–231. <https://doi.org/10.1016/j.gca.2012.10.058>.
- Dahl, T.W., Connelly, J.N., Li, D., Kouchinsky, A., Gill, B.C., Porter, S., Maloof, A.C., Bizzarro, M., 2019. Atmosphere-ocean oxygen and productivity dynamics during

- early animal radiations. Proc. Natl. Acad. Sci. 116, 19352–19361. <https://doi.org/10.1073/pnas.1901178116>.
- Damanik, A., Wille, M., Ahmad, Q., Chatterjee, S., Crowe, S.A., Bauer, K.W., Grosjean, M., Cahyarini, S.Y., Bijaksana, S., Russell, J.M., Vogel, H., 2024. Low Mo mobility during the laterization of ultramafic bedrock: evidence from the East Sulawesi ophiolite, Indonesia. Chem. Geol. 660, 122150. <https://doi.org/10.1016/j.chemgeo.2024.122150>.
- Duan, Y., Anbar, A.D., Arnold, G.L., Lyons, T.W., Gordon, G.W., Kendall, B., 2010. Molybdenum isotope evidence for mild environmental oxygenation before the Great Oxidation Event. Geochem. Cosmochim. Acta 74, 6655–6668. <https://doi.org/10.1016/j.gca.2010.08.035>.
- Fan, J.-J., Li, J., Wang, Q., Zhang, L., Zhang, J., Zeng, X.-L., Ma, L., Wang, Z.-L., 2020. High-precision molybdenum isotope analysis of low-Mo igneous rock samples by MC-ICP-MS. Chem. Geol. 545, 119648. <https://doi.org/10.1016/j.chemgeo.2020.119648>.
- Feng, L., Zhou, L., Hu, W., Zhang, W., Li, B., Liu, Y., Hu, Z., Yang, L., 2020. A simple single-stage extraction method for Mo separation from geological samples for isotopic analysis by MC-ICP-MS. J. Anal. At. Spectrom. 35, 145–154. <https://doi.org/10.1039/C9JA00267G>.
- Friese, A., Bauer, K., Glombitza, C., Ordoñez, L., Ariztegui, D., Heuer, V.B., Vuillemin, A., Henrey, C., Nomosatryo, S., Simister, R., Wagner, D., Bijaksana, S., Vogel, H., Melles, M., Russell, J.M., Crowe, S.A., Kallmeyer, J., 2021. Organic matter mineralization in modern and ancient ferruginous sediments. Nat. Commun. 12, 2216. <https://doi.org/10.1038/s41467-021-22453-0>.
- Fukushima, T., Matsushita, B., Subehi, L., Setiawan, F., Wibowo, H., 2017. Will hypolimnetic waters become anoxic in all deep tropical lakes? Sci. Rep. 7, 45320. <https://doi.org/10.1038/srep45320>.
- Goldberg, S., Forster, H.S., Godfrey, C.L., 1996. Molybdenum adsorption on oxides, clay minerals, and soils. Soil Sci. Soc. Am. J. 60, 425–432. <https://doi.org/10.2136/sssaj1996.03615995006000020013x>.
- Goldberg, T., Archer, C., Vance, D., Poultton, S.W., 2009. Mo isotope fractionation during adsorption to Fe (oxyhydr)oxides. Geochem. Cosmochim. Acta 73, 6502–6516. <https://doi.org/10.1016/j.gca.2009.08.004>.
- Goldberg, T., Archer, C., Vance, D., Thamdrup, B., McAnena, A., Poultton, S.W., 2012. Controls on Mo isotope fractionations in a Mn-rich anoxic marine sediment, Gullmar Fjord, Sweden. Chem. Geol. 296–297, 73–82. <https://doi.org/10.1016/j.chemgeo.2011.12.020>.
- Goldberg, T., Gordon, G., Izon, G., Archer, C., Pearce, C.R., McManus, J., Anbar, A.D., Rehkämper, M., 2013. Resolution of inter-laboratory discrepancies in Mo isotope data: an intercalibration. J. Anal. At. Spectrom. 28, 724–735. <https://doi.org/10.1039/c3ja30375f>.
- Golightly, J.P., 1979. The chemical composition and infrared spectrum of nickel- and iron-substituted serpentine from a nickeliferous laterite profile. Soroako, Indonesia. Gebre, N.D., Siebert, C., Nägler, T.F., Pettke, T., 2012. δ⁹⁸/⁹⁵Mo values and molybdenum concentration data for NIST SRM 610, 612 and 3134: towards a common protocol for reporting Mo data. Geostand. Geoanal. Res. 36, 291–300. <https://doi.org/10.1111/j.1751-908X.2012.00160.x>.
- Hardisty, D.S., Riedinger, N., Planavsky, N.J., Asael, D., Andren, T., Jorgensen, B.B., Lyons, T.W., 2016. A Holocene history of dynamic water column redox conditions in the Landsort Deep, Baltic Sea. Am. J. Sci. 316, 713–745. <https://doi.org/10.2475/08.2016.01>.
- Hasberg, A.K.M., Bijaksana, S., Held, P., Just, J., Melles, M., Morlock, M.A., Opitz, S., Russell, J.M., Vogel, H., Wennrich, V., 2019. Modern sedimentation processes in Lake Towuti, Indonesia, revealed by the composition of surface sediments. Sedimentology 66, 675–698. <https://doi.org/10.1111/sed.12503>.
- Helz, G.R., Bura-Nakić, E., Mikac, N., Ciglanečki, I., 2011. New model for molybdenum behavior in euxinic waters. Chem. Geol. 284, 323–332. <https://doi.org/10.1016/j.chemgeo.2011.03.012>.
- Janssen, D.J., Damanik, A., Tournier, N., Tolu, J., Winkel, L., Cahyarini, S.Y., Vogel, H., 2024. Biogeochemical cycling of trace elements and nutrients in ferruginous waters: constraints from a deep oligotrophic ancient lake. Limnol. Oceanogr. 12687. <https://doi.org/10.1002/lno.12687> Ino.
- Kadarusman, A., Miyashita, S., Maruyama, S., Parkinson, C.D., Ishikawa, A., 2004. Petrology, geochemistry and paleogeographic reconstruction of the East Sulawesi ophiolite, Indonesia. Tectonophysics 392, 55–83. <https://doi.org/10.1016/j.tecto.2004.04.008>.
- Kashiwabara, T., Takahashi, Y., Tanimizu, M., Usui, A., 2011. Molecular-scale mechanisms of distribution and isotopic fractionation of molybdenum between seawater and ferromanganese oxides. Geochem. Cosmochim. Acta 75, 5762–5784. <https://doi.org/10.1016/j.gca.2011.07.022>.
- Katsev, S., Crowe, S.A., Mucci, A., Sundby, B., Nomosatryo, S., Douglas Haffner, G., Fowle, D.A., 2010. Mixing and its effects on biogeochemistry in the persistently stratified, deep, tropical Lake Matano, Indonesia. Limnol. Oceanogr. 55, 763–776. <https://doi.org/10.4319/lo.2010.55.2.0763>.
- Kendall, B., Dahl, T.W., Anbar, A.D., 2017. The stable isotope geochemistry of molybdenum. Rev. Mineral. Geochem. 22, 683–732. <https://doi.org/10.2138/rmg.2017.82.16>.
- King, E.K., Peralis, S.S., Pett-Ridge, J.C., 2018. Molybdenum isotope fractionation during adsorption to organic matter. Geochem. Cosmochim. Acta 222, 584–598. <https://doi.org/10.1016/j.gca.2017.11.014>.
- Konecky, B., Russell, J., Bijaksana, S., 2016. Glacial aridity in central Indonesia coeval with intensified monsoon circulation. Earth Planet Sci. Lett. 437, 15–24. <https://doi.org/10.1016/j.epsl.2015.12.037>.
- Kurzweil, F., Drost, K., Pašava, J., Wille, M., Taubald, H., Schoeckle, D., Schoenberg, R., 2015. Coupled sulfur, iron and molybdenum isotope data from black shales of the Teplá-Barrandian unit argue against deep ocean oxygenation during the Ediacaran. Geochim. Cosmochim. Acta 171, 121–142. <https://doi.org/10.1016/j.gca.2015.08.022>.
- Lehmusluoto, P., Machhub, B., 1997. National inventory of the major lakes and reservoirs in Indonesia: general limnology. Rev. Research Institute for Water Resources Development, Ministry of Public Works, Agency for Research and Development ; Dept. Of Limnology and Environmental Protection. University of Helsinki, Faculty of Agriculture and Forestry, Bandung : Helsinki.
- Lyons, T.W., Reinhard, C.T., Planavsky, N.J., 2014. The rise of oxygen in Earth's early ocean and atmosphere. Nature 506, 307–315. <https://doi.org/10.1038/nature13068>.
- Makri, S., Wienhues, G., Bigalke, M., Gilli, A., Rey, F., Tinner, W., Vogel, H., Grosjean, M., 2021. Variations of sedimentary Fe and Mn fractions under changing lake mixing regimes, oxygenation and land surface processes during Late-glacial and Holocene times. Sci. Total Environ. 755, 143418. <https://doi.org/10.1016/j.scitotenv.2020.143418>.
- Malinovsky, D., Hammarlund, D., Ilyashuk, B., Martinsson, O., Gelting, J., 2007. Variations in the isotopic composition of molybdenum in freshwater lake systems. Chem. Geol. 236, 181–198. <https://doi.org/10.1016/j.chemgeo.2006.09.006>.
- Morlock, M.A., Vogel, H., Nigg, V., Ordonez, L., Hasberg, A.K.M., Melles, M., Russell, J.M., Bijaksana, S., the TDP Science Team, 2019. Climatic and tectonic controls on source-to-sink processes in the tropical, ultramafic catchment of Lake Towuti, Indonesia. J. Paleolimnol. 61, 279–295. <https://doi.org/10.1007/s10933-018-0059-3>.
- Nägler, T.F., Neubert, N., Böttcher, M.E., Dellwig, O., Schnetger, B., 2011. Molybdenum isotope fractionation in pelagic euxinia: evidence from the modern Black and Baltic Seas. Chem. Geol. 289, 1–11. <https://doi.org/10.1016/j.chemgeo.2011.07.001>.
- Neubert, N., Nägler, T.F., Böttcher, M.E., 2008. Sulfitid controls molybdenum isotope fractionation into euxinic sediments: evidence from the modern Black Sea. Geology 36 (1), 775. <https://doi.org/10.1130/G24959A>.
- Ossa Ossa, F., Hofmann, A., Wille, M., Spangenberg, J.E., Bekker, A., Poulton, S.W., Eickmann, B., Schoenberg, R., 2018. Aerobic iron and manganese cycling in a redox-stratified Mesoarchean epicontinent sea. Earth Planet Sci. Lett. 500, 28–40. <https://doi.org/10.1016/j.epsl.2018.07.044>.
- Parish, M., Russell, J., Konecky, B., Du, X., He, C., Bijaksana, S., Vogel, H., 2024. Changes in Indo-Pacific Warm Pool hydroclimate and vegetation during the last deglaciation. Quat. Sci. Rev. 336, 108755. <https://doi.org/10.1016/j.quascirev.2024.108755>.
- Parish, M.C., Du, X., Bijaksana, S., Russell, J.M., 2023. A brGDGT-based reconstruction of terrestrial temperature from the maritime continent spanning the last glacial maximum. Paleoceanogr. Paleoclimatol. 38, e2022PA004501. <https://doi.org/10.1029/2022PA004501>.
- Pearce, C.R., Cohen, A.S., Coe, A.L., Burton, K.W., 2008. Molybdenum isotope evidence for global ocean anoxia coupled with perturbations to the carbon cycle during the Early Jurassic. Geology 36 (1), 231. <https://doi.org/10.1130/G24446A>.
- Planavsky, N.J., Asael, D., Hofmann, A., Reinhard, C.T., Lalonde, S.V., Knudsen, A., Wang, X., Ossa Ossa, F., Peccoits, E., Smith, A.J.B., Beukes, N.J., Bekker, A., Johnson, T.M., Konhauser, K.O., Lyons, T.W., Rouxel, O.J., 2014. Evidence for oxygenic photosynthesis half a billion years before the Great Oxidation Event. Nat. Geosci. 7, 283–286. <https://doi.org/10.1038/ngeo2122>.
- Planavsky, N.J., McGoldrick, P., Scott, C.T., Li, C., Reinhard, C.T., Kelly, A.E., Chu, X., Bekker, A., Love, G.D., Lyons, T.W., 2011. Widespread iron-rich conditions in the mid-Proterozoic ocean. Nature 477, 448–451. <https://doi.org/10.1038/nature13027>.
- Poulton, R.L., Siebert, C., McManus, J., Berelson, W.M., 2006. Authigenic molybdenum isotope signatures in marine sediments. Geology 34, 617. <https://doi.org/10.1130/G22485.1>.
- Poulton, S.W., Canfield, D.E., 2011. Ferruginous conditions: a dominant feature of the ocean through Earth's history. Elements 7, 107–112. <https://doi.org/10.2113/gselements.7.2.107>.
- Pu, T., Haffner, G., Crowe, S., Katsev, S., 2025. Stratification stability of tropical lakes and their sensitivity to climate. Limnol. Oceanogr. n/a-n/a. <https://doi.org/10.1002/lno.70055>.
- Russell, J.M., Vogel, H., Bijaksana, S., Melles, M., Deino, A., Hafidz, A., Haffner, D., Hasberg, A.K.M., Morlock, M., Von Rintelen, T., Sheppard, R., Stelbrink, B., Stevenson, J., 2020. The late quaternary tectonic, biogeochemical, and environmental evolution of ferruginous Lake Towuti, Indonesia. Palaeogeogr. Palaeoclimatol. Palaeoecol. 556, 109905. <https://doi.org/10.1016/j.palaeo.2020.109905>.
- Russell, J.M., Vogel, H., Konecky, B.L., Bijaksana, S., Huang, Y., Melles, M., Watrus, N., Costa, K., King, J.W., 2014. Glacial forcing of central Indonesian hydroclimate since 60. 000 y B.P. Proc. Natl. Acad. Sci. 111, 5100–5105. <https://doi.org/10.1073/pnas.1402373111>.
- Scholz, F., Baum, M., Siebert, C., Eroglu, S., Dale, A.W., Naumann, M., Sommer, S., 2018. Sedimentary molybdenum cycling in the aftermath of seawater inflow to the intermittently euxinic Gotland Deep, Central Baltic Sea. Chem. Geol. 491, 27–38. <https://doi.org/10.1016/j.chemgeo.2018.04.031>.
- Scholz, F., Siebert, C., Dale, A.W., Frank, M., 2017. Intense molybdenum accumulation in sediments underneath a nitrogenous water column and implications for the reconstruction of paleo-redox conditions based on molybdenum isotopes. Geochem. Cosmochim. Acta 213, 400–417. <https://doi.org/10.1016/j.gca.2017.06.048>.
- Scott, C., Lyons, T.W., 2012. Contrasting molybdenum cycling and isotopic properties in euxinic versus non-euxinic sediments and sedimentary rocks: refining the paleoproxies. Chem. Geol., Special Issue Recent Advances in Trace Metal Applications to Paleoceanographic Studies 324–325, 19–27. <https://doi.org/10.1016/j.chemgeo.2012.05.012>.

- Scott, C., Lyons, T.W., Bekker, A., Shen, Y., Poulton, S.W., Chu, X., Anbar, A.D., 2008. Tracing the stepwise oxygenation of the Proterozoic ocean. *Nature* 452, 456–459. <https://doi.org/10.1038/nature06811>.
- Sheppard, R.Y., Milliken, R.E., Russell, J.M., Dyar, M.D., Sklute, E.C., Vogel, H., Melles, M., Bijaksana, S., Morlock, M.A., Hasberg, A.K.M., 2019. Characterization of iron in Lake Towuti sediment. *Chem. Geol.* 512, 11–30. <https://doi.org/10.1016/j.chemgeo.2019.02.029>.
- Siebert, C., Kramers, J.D., Meisel, Th., Morel, Ph., Nägler, ThF., 2005. PGE, Re-Os, and Mo isotope systematics in Archean and early Proterozoic sedimentary systems as proxies for redox conditions of the early Earth. *Geochim. Cosmochim. Acta* 69, 1787–1801. <https://doi.org/10.1016/j.gca.2004.10.006>.
- Siebert, C., Nägler, T.F., Kramers, J.D., 2001. Determination of molybdenum isotope fractionation by double-spike multicollector inductively coupled plasma mass spectrometry. *G-cubed* 2, 2000GC000124. <https://doi.org/10.1029/2000GC000124>.
- Siebert, C., Nägler, T.F., Von Blanckenburg, F., Kramers, J.D., 2003. Molybdenum isotope records as a potential new proxy for paleoceanography. *Earth Planet Sci. Lett.* 211, 159–171. [https://doi.org/10.1016/S0012-821X\(03\)00189-4](https://doi.org/10.1016/S0012-821X(03)00189-4).
- Siebert, C., Scholz, F., Kuhnt, W., 2021. A new view on the evolution of seawater molybdenum inventories before and during the Cretaceous Oceanic Anoxic Event 2. *Chem. Geol.* 582, 120399. <https://doi.org/10.1016/j.chemgeo.2021.120399>.
- Swanner, E.D., Lambrecht, N., Wittkop, C., Harding, C., Katsev, S., Torgeson, J., Poulton, S.W., 2020. The biogeochemistry of ferruginous lakes and past ferruginous oceans. *Earth Sci. Rev.* 211, 103430. <https://doi.org/10.1016/j.earscirev.2020.103430>.
- Tournier, N., Fabbri, S.C., Anselmetti, F.S., Cahyarini, S.Y., Bijaksana, S., Watrus, N., Russell, J.M., Vogel, H., 2023. Climate-controlled sensitivity of lake sediments to record earthquake-related mass wasting in tropical Lake Towuti during the past 40 kyr. *Quat. Sci. Rev.* 305, 108015. <https://doi.org/10.1016/j.quascirev.2023.108015>.
- Trivobillard, N., Algeo, T.J., Lyons, T., Ribouleau, A., 2006. Trace metals as paleoredox and paleoproductivity proxies: an update. *Chem. Geol.* 232, 12–32. <https://doi.org/10.1016/j.chemgeo.2006.02.012>.
- Voegelin, A.R., Nägler, T.F., Beukes, N.J., Lacassie, J.P., 2010. Molybdenum isotopes in late Archean carbonate rocks: implications for early Earth oxygenation. *Precambr. Res.* 182, 70–82. <https://doi.org/10.1016/j.precamres.2010.07.001>.
- Vogel, H., Russell, J.M., Cahyarini, S.Y., Bijaksana, S., Watrus, N., Rethemeyer, J., Melles, M., 2015. Depositional modes and lake-level variability at Lake Towuti, Indonesia, during the past ~29 kyr BP. *J. Paleolimnol.* 54, 359–377. <https://doi.org/10.1007/s10933-015-9857-z>.
- Vuillemin, A., Friese, A., Alawi, M., Henny, C., Nomosatryo, S., Wagner, D., Crowe, S.A., Kallmeyer, J., 2016. Geomicrobiological features of ferruginous sediments from Lake Towuti, Indonesia. *Front. Microbiol.* 7. <https://doi.org/10.3389/fmicb.2016.01007>.
- Vuillemin, A., Mayr, C., Schuessler, J.A., Friese, A., Bauer, K.W., Lücke, A., Heuer, V.B., Glombitsa, C., Henny, C., Bijaksana, S., Vogel, H., Crowe, S.A., Kallmeyer, J., 2022. A one-million-year isotope record from siderites formed in modern ferruginous sediments. *Geol. Soc. Am. Bull.* 130.
- Wang, Z., Ma, J., Li, J., Zeng, T., Zhang, Z., He, X., Zhang, L., Wei, G., 2020. Effect of Fe–Ti oxides on Mo isotopic variations in lateritic weathering profiles of basalt. *Geochim. Cosmochim. Acta* 286, 380–403. <https://doi.org/10.1016/j.gca.2020.07.030>.
- Wicaksono, S.A., Russell, J.M., Bijaksana, S., 2015. Compound-specific carbon isotope records of vegetation and hydrologic change in central Sulawesi, Indonesia, since 53,000 yr BP. *Palaeogeogr. Palaeoclimatol. Palaeoecol.* 430, 47–56. <https://doi.org/10.1016/j.palaeo.2015.04.016>.
- Willbold, M., Hibbert, K., Lai, Y.-J., Freymuth, H., Hin, R.C., Coath, C., Vils, F., Elliott, T., 2016. High-Precision mass-dependent molybdenum isotope variations in magmatic rocks determined by double-spike MC-ICP-MS. *Geostand. Geoanal. Res.* 389–403. <https://doi.org/10.1111/ggr.12109>.
- Wille, M., Kramers, J.D., Nägler, T.F., Beukes, N.J., Schröder, S., Meisel, Th., Lacassie, J.P., Voegelin, A.R., 2007. Evidence for a gradual rise of oxygen between 2.6 and 2.5 Ga from Mo isotopes and Re-PGE signatures in shales. *Geochim. Cosmochim. Acta* 71, 2417–2435. <https://doi.org/10.1016/j.gca.2007.02.019>.
- Wille, M., Nebel, O., Van Kranendonk, M.J., Schoenberg, R., Kleinhanns, I.C., Ellwood, M.J., 2013. Mo–Cr isotope evidence for a reducing Archean atmosphere in 3.46–2.76 Ga black shales from the Pilbara, Western Australia. *Chem. Geol.* 340, 68–76. <https://doi.org/10.1016/j.chemgeo.2012.12.018>.
- Wirth, S.B., Gilli, A., Niemann, H., Dahl, T.W., Ravasi, D., Sax, N., Hamann, Y., Peduzzi, R., Peduzzi, S., Tonolla, M., Lehmann, M.F., Anselmetti, F.S., 2013. Combining sedimentological, trace metal (Mn, Mo) and molecular evidence for reconstructing past water-column redox conditions: the example of meromictic Lake Cadagno (Swiss Alps). *Geochim. Cosmochim. Acta* 120, 220–238. <https://doi.org/10.1016/j.gca.2013.06.017>.
- Zander, P.D., Żarczyński, M., Vogel, H., Tylmann, W., Wacnik, A., Sanchini, A., Grosjean, M., 2021. A high-resolution record of Holocene primary productivity and water-column mixing from the varved sediments of Lake Żabińskie, Poland. *Sci. Total Environ.* 755, 143713. <https://doi.org/10.1016/j.scitotenv.2020.143713>.
- Zhao, B., Russell, J.M., Tsai, V.C., Blaus, A., Parish, M.C., Liang, J., Wilk, A., Du, X., Bush, M.B., 2023. Evaluating global temperature calibrations for lacustrine branched GDGTs: seasonal variability, paleoclimate implications, and future directions. *Quat. Sci. Rev.* 310, 108124. <https://doi.org/10.1016/j.quascirev.2023.108124>.
- Zhao, P., Li, J., Zhang, L., Wang, Z., Kong, D., Ma, J., Wei, G., Xu, J., 2016. Molybdenum mass fractions and isotopic compositions of international geological reference materials. *Geostand. Geoanalytical Res.* 40, 217–226. <https://doi.org/10.1111/j.1751-908X.2015.00373.x>.